Journal of Neuroinflammation

RESEARCH

Open Access

Alterations of the *IKZF1-IKZF2* tandem in immune cells of schizophrenia patients regulate associated phenotypes

Iván Ballasch[1,2,3†], Laura López-Molina[1,2,3†], Marcos Galán-Ganga[1,2,3], Anna Sancho-Balsells[1,2,3], Irene Rodríguez-Navarro[1,2,3], Sara Borràs-Pernas[1,2,3], M. Angeles Rabadan[4], Wanqi Chen[1,2,3], Carlota Pastó-Pellicer[1,2,3], Francesca Flotta[1,2,3], Wang Maoyu[1,2,3], Joaquín Fernández-Irigoyen[5], Enrique Santamaría[5], Ruth Aguilar[6], Carlota Dobaño[6,7], Natalia Egri[8], Carla Hernandez[10], Miqueu Alfonso[10], Manel Juan[1,8,9], Jordi Alberch[1,2,3,11], Daniel del Toro[1,2,3], Belén Arranz[10], Josep M. Canals[1,2,3,11] and Albert Giralt[1,2,3,11*]

Abstract

Schizophrenia is a complex multifactorial disorder and increasing evidence suggests the involvement of immune dysregulations in its pathogenesis. We observed that *IKZF1* and *IKZF2*, classic immune-related transcription factors (TFs), were both downregulated in patients' peripheral blood mononuclear cells (PBMCs) but not in their brain. We generated a new mutant mouse model with a reduction in *Ikzf1* and *Ikzf2* to study the impact of those changes. Such mice developed deficits in the three dimensions (positive–negative-cognitive) of schizophrenia-like phenotypes associated with alterations in structural synaptic plasticity. We then studied the secretomes of cultured PBMCs obtained from patients and identified potentially secreted molecules, which depended on *IKZF1* and *IKZF2* mRNA levels, and that in turn have an impact on neural synchrony, structural synaptic plasticity and schizophrenia-like symptoms in in vivo and in vitro models. Our results point out that *IKZF1-IKZF2*-dependent immune signals negatively impact on essential neural circuits involved in schizophrenia.

Keywords IL-4, CXCL10, CCL5, Neuronal networks, Ikaros, Helios, Lymphocytes, Mouse models, Cognitive symptoms, Negative symptoms

†Iván Ballasch and Laura López-Molina have contributed equally.

*Correspondence:
Albert Giralt
albertgiralt@ub.edu
[1] Departament de Biomedicina, Facultat de Medicina, Institut de Neurociències, Universitat de Barcelona, 08036 Barcelona, Spain
[2] Institut d'Investigacions Biomèdiques August Pi i Sunyer (IDIBAPS), 08036 Barcelona, Spain
[3] Centro de Investigación Biomédica en Red Sobre Enfermedades Neurodegenerativas (CIBERNED), 28031 Madrid, Spain
[4] ZeClinics SL. and ZeNeuroid SL., Barcelona, Spain
[5] Proteomics Platform, Navarrabiomed, Hospital Universitario de Navarra (HUN), Universidad Pública de Navarra UPNA, IdiSNA, 31008 Pamplona, Spain
[6] ISGlobal, Hospital Clínic – Universitat de Barcelona, Barcelona, Catalonia, Spain
[7] CIBER Enfermedades Infecciosas (CIBERINFEC), Barcelona, Catalonia, Spain
[8] Servei d'Immunologia, Hospital Clinic Barcelona (HCB) - CDB, Fundació Clínic de Recerca Biomèdica - IDIBAPS, Barcelona, Spain
[9] Plataforma d'Immunoteràpia HSJD-HCB, Barcelona, Spain
[10] Parc Sanitari Sant Joan de Déu, CIBERSAM, Barcelona, Spain
[11] Production and Validation Centre of Advanced Therapies (Creatio), Faculty of Medicine and Health Science, University of Barcelona, 08036 Barcelona, Spain

Introduction

Schizophrenia is composed of a myriad of heterogeneous symptoms that challenges a unified description of the disease. This represents a global burden, as schizophrenia ranks within the top 10 causes of disabilities in developed countries, with 24 million people affected worldwide (GHDx). Furthermore, due to its early age of onset of 16–25 years [62, 79], the disease results in more than 12 million disability-adjusted life years annually. Behavioral signatures of schizophrenia are broadly divided into three categories: (1) positive symptoms (delusions and hallucinations); (2) negative symptoms (lack of pleasure, social withdrawal), and (3) cognitive symptoms (impairment of short-term working memory, attention deficit). Current treatments only provide some symptomatic relief for positive symptoms whereas treatments for cognitive and negative symptoms remain elusive [75]. Notably, cognitive and negative symptoms are responsible for a major proportion of the disability associated with schizophrenia and are more constant over time [75, 95]. Also, the current lack of insight into the disease is not only due to the heterogeneity of the symptomatology [74], but also due to the complexity of the causative factors underlying the disease, including genetic and immunological [17]. Therefore, what is urgently needed are novel mechanistic insights into the molecular paths underlying the negative and cognitive symptomatology subtypes of the disorder.

Although schizophrenia has been classically observed as a brain disease, current evidence points towards a multi-system network underlying positive, negative, and cognitive symptoms [12, 99]. In this sense, the communication between the immune and central nervous systems has already been described to be altered in schizophrenia [65]. As illustrative example, it has been shown that lymphocyte invasion is higher in patients with prevalence of negative symptomatology [9] and that levels of inflammatory cytokines (TNF-a and IL-6 or C-reactive protein) correlate with negative and cognitive symptoms in schizophrenia [31, 45, 52]. However, what we know so far is reduced to the description of circulating molecules that probably serve as a molecular bridge between these two systems [77]. Major mechanistic insights are still lacking, especially regarding the regulation of these molecules, their aberrant release, and the specific targeted neural circuits they affect. In this line, a highly promising target as a molecular bridge between the neural and immune system is the Ikaros family of transcription factors (TFs), which include Ikaros zinc finger 1 (*IKZF1* or Ikaros) and Ikaros zinc finger 2 (*IKZF2* or Helios). These TFs have been largely described to be crucial for the normal development of immune cells (T-cells, B-cells, and monocytes) [27] and their function (e.g. production of *mb-1*, *CD3*, *IL2*, *IL4*, and *NFkB* among others [64]. Furthermore, evidence starts to emerge, that they could play an important role in schizophrenia. For instance, specific *IKZF1* single nucleotide polymorphisms (SNPs) such as rs7805803 and rs10276619 have been associated with changes in brain and ventricle volumes [23] and with hippocampal atrophy [69], respectively—neuropathological features heavily implicated in schizophrenia [38]. Additionally, *IKZF1* mutations such as rs116427960 and rs186807222 have been linked to schizophrenia and associated executive function deficits [14, 40]. *IKZF1* levels have also been related with the age of onset of schizophrenia [78]. Regarding *IKZF2*, evidence, although more limited, highlights its relevance. *IKZF2* levels are highly sensitive to treatment with lipopolysaccharides (LPS), a widely used experimental model for schizophrenia [25]. Moreover, Helios deficiency results in overexpression of WDFY1, an immune scaffold protein commonly elevated in schizophrenia patients [81]. Finally, *IKZF2* dysregulation has been observed in individuals with autism spectrum disorder [2, 4], a condition frequently co-occurring with psychosis. Nevertheless, the function of the *IKZF* family in the communication between the immune and neural systems during the development of schizophrenia is practically unexplored.

In the present work, we hypothesized that immune alterations in schizophrenia could be associated with altered mRNA levels (and function) of *IKZF1* and *IKZF2*, and that these potential changes could impact the communication between the immune and central nervous systems during the progression of the disorder. To address this hypothesis, we first confirmed the altered state of the two transcription factors in human samples (brain and circulating immune cells). Subsequently, to validate their specificity and biological relevance, we used genetically modified mice devoid of *Ikzf1*, *Ikzf2*, or both. Finally, to evaluate the aberrant communication between the immune and central nervous systems, we transferred the secretome of human circulating immune cells (PBMCs) into the brains of living mice. In these mice, we evaluated whether schizophrenia-like phenotypes were induced in terms of behavior and histological markers.

Materials and methods

Human post-mortem brain samples

The brain samples from schizophrenia (SCH) patients used in this study were provided by the Sant Joan de Déu Brain Bank (Sant Boi de Llobregat, Barcelona, Spain). The donation and obtention of samples were regulated by the ethics committee of the institution. The sample processing followed the rules of the European Consortium of Nervous Tissues: BrainNet Europe II (BNEII). All the samples were protected in terms of individual donor identification following the BNEII laws. Clinical

diagnosis of SCH in donor subjects was confirmed premortem with DMS-IV (Diagnostic and Statistical Manual of Mental Disorders—4th edition) and ICD-10 (International Statistical Classification of Diseases and Related Health Problems) criteria by clinical examiners. Most donors were hospitalized for more than 40 years and were re-evaluated every 2 years to monitor and update their clinical progression. Case information can be found in Supplementary Table 1. Control samples (hippocampus, putamen, and dorsolateral prefrontal cortex) were obtained from Banc de Teixits Neurològics (Servei Científico-Tècnics, Universitat de Barcelona, Barcelona, Spain) and the sample processing also followed the BNEII rules. Case information can be also found in Supplementary Table 1. All the procedures for the obtention of post-mortem samples followed the ethical guidelines of the Declaration of Helsinki and local ethical committees (Universitat de Barcelona: IRB00003099; Fundació CEIC Sant Joan de Déu: BTN-PSSJD, CER122306).

Immunoblotting

The tissue was lysed by sonication in 250 µl of lysis buffer as described elsewhere [28]. After lysis, samples were centrifuged at 12,000 r.p.m. for 20 min. Supernatant proteins (15 µg) from total brain region extracts were loaded in SDS–PAGE and transferred to nitrocellulose membranes (GE Healthcare, LC, UK). Membranes were blocked in TBS-T (150 mM NaCl, 20 mM Tris–HCl, pH 7.5, 0.5 ml Tween 20) with 50 g l−1 non-fat dry milk and 50 g l−1 BSA. Immunoblots were probed with the following antibodies: anti-Ikzf1 (1:1000, D6N9Y, Cell Signaling Technology, Danvers, MA, USA,#14859), anti-Ikzf2 (1:1000, GeneTex, California. USA, #GTX115630). All blots were incubated with the primary antibody overnight at 4 °C by shaking in PBS with 0.2 g l−1 sodium azide. After three washes in TBS-T, blots were incubated for 1 h at room temperature with the corresponding horseradish peroxidase-conjugated antibody (1:2000; Promega, Madison, WI, USA) and washed again with TBS-T. Immunoreactive bands were visualized using the Western Blotting Luminol Reagent (Santa Cruz Biotechnology, #sc-2048) and quantified by a computer-assisted densitometer (Gel-Pro Analyzer, version 4, Media Cybernetics). For loading control, a mouse monoclonal antibody for actin was used (1:20,000; MP Biochemicals, #0869100-CF).

Recruitment of patients

The sample of this study (N◦PI17/00246, PI Belen Arranz) was recruited in the Outpatient clinic located in Cornellà, Barcelona, Spain (Parc Sanitari Sant Joan de Deu). Adult controls and patients with DSM-5 (Diagnostic and Statistical Manual of Mental Disorders) schizophrenia-spectrum disorder at any stage of the disease were included. The inclusion criteria for patients were: (1) adults over 18 years of age; (2) ability to speak Spanish correctly; and (3) signed informed consent. Exclusion criteria were: (1) history of head trauma with loss of consciousness and (2) organic disease with mental repercussions; (3) presence of an acute inflammatory process: (3.1) fever (> 38◦C) or infection in the 2 weeks prior to the baseline interview, or (3.2) have received vaccinations in the past 4 weeks. This study was conducted following the ethical principles of the Declaration of Helsinki and Good Clinical Practice and the Ethics and Research Board from Parc Sanitari Sant Joan de Deu. All participants provided written informed consent prior to their inclusion in the study. Case information can be found in Supplementary Table 2.

Human peripheral blood mononuclear cells (PBMCs) and isolation of CD4 + and CD8 + cells

Human peripheral blood mononuclear cells (PBMCs) were isolated from peripheral blood. The cell fraction corresponding to red blood cells and granulocytes (neutrophils, basophils, and eosinophils) was removed from whole blood by density gradient centrifugation as described elsewhere [47]. For this procedure, 10 ml blood samples were diluted with 10 ml of phosphate-buffered saline (PBS) pH-7.2. Consequently, 10 ml of diluted blood were placed in 15 ml tubes filled with 4 ml of a density gradient medium with $\rho = 1.077$ g/ml (e.g. Ficoll-Paque PLUS) and centrifuged at $500 \times g$ for 35 min at 20 °C without brake. PBMCs were then transferred to 50 ml tubes, the tubes were filled with PBS and centrifuged at $500 \times g$ for 10 min at 20 °C. PBMCs were then lysated for mRNA (see next section) or plated. For PBMCs plating, after elimination of the supernatant, PBMCs were resuspended in X-vivo medium (#BEBP02-055Q Lonza bioscience, Maryland, USA) supplemented with pen/strep 1%/1%, L-glutamine 1% and Hepes 0,02 M. Cells were seeded in 24-well plates (1 ml per well at $4 \cdot 10^6$ cells/ml) and left in an incubator at 37 °C, 5% CO2. After 24 h, PBMCs were treated with PMA (50 ng/ml, #P1585, Sigma-Aldrich Chemical Co., St. Louis, MO, USA) and Ionomycin (1 µM, #I0634 Sigma-Aldrich Chemical Co.) for 6 h, then we centrifuged the cultures to take separately the supernatant and the pellet, both were stored at − 80 °C. For the CD4 + and CD8 + isolation the Pan T Cell Isolation Kit was used to isolate T cells from human PBMC previously obtained through negative selection following manufacturer's instructions (Miltenyi, Cat. #130-096-535). T cells were then subjected to further magnetic labeling and separation to isolate CD4 + and CD8 + cells. First, T cells were incubated with CD8 MicroBeads (Miltenyi, Cat. #130-045-201) for 15 min at

4 °C and cell suspension was applied onto the magnetic columns. The flow-through containing unlabeled cells was collected and considered the CD4 + enriched fraction. Then, labeled CD8 + cells were removed from the column with buffer. Both fractions were centrifuged at 300 *g* × 7 min and the final cellular pellets were lysed with the proper buffer for subsequent RNA extraction.

mRNA extraction and RT-qPCR

PBMCs were homogenized and total RNA was extracted using PureLink RNA Micro Scale kit (#12183-016, Invitrogen) according to manufacturer's recommendations. RNA purity and quantity were determined with Nanodrop 1000 spectrophotometer (Thermo Fisher). 500 ng of purified RNA was reverse transcribed using the High Capacity cDNA Reverse Transcription Kit (Applied Biosystems, Cat. #436814). The cDNA synthesis was performed at 25 °C for 10 min, at 37 °C for 120 min and a final step at 85 °C for 5 min in a final volume of 20 µl as instructed by manufacturer. Then, cDNA was analyzed by quantitative RT-PCR using PrimeTime qPCR Assays (Integrated DNA Technologies, Coralville, Iowa. USA). Human assays: IKZF1 (Hs.PT.58.25575505), IKZF2 (Hs.PT.58.2960172), and 18S (Hs.PT.39a.22214856.g). Mouse assays: IKZF1 (Hs.PT.58.25575505), IKZF2 (Hs.PT.58.2960172) and 18S (Hs.PT.39a.22214856.g). Quantitative PCR was performed in 12 µl of final volume on 96-well plates using the Premix Ex Taq (Takara Biotechnology, #RR037A). Reactions included Segment 1: 1 cycle of 30 s at 95 °C and Segment 2: 40 cycles of 5 s at 95 °C and 20 s at 60 °C. All RT-PCR assays were run in duplicate. To provide negative control and exclude contamination by genomic DNA, the PrimeScript RT enzyme was omitted in the cDNA synthesis step and samples were subjected to the PCR reaction in the same manner with each probe. RT-PCR data were quantified using the comparative quantitation analysis program of 64 MxProTM quantitative PCR software version 3.0 (Stratagene) and 18S gene expression was used as housekeeping gene. To analyze the relative changes in gene expression, the 2(−ΔΔ C(T)) method was used.

Treatments with antipsychotics in mice

Female and male adult (12-week-old) wild type mice (C57BL/6 J strain) were purchased from Jackson Laboratory (Cat. #000664). All mice (male and female, 50% each) were sub-chronically (7 days) or chronically (28 days, only for clozapine) treated (i.p.) with vehicle or paliperidone (0.5 mg/Kg dissolved in PBS, 5% DMSO) or clozapine (1 mg/Kg dissolved in PBS, 5% DMSO). Doses were used following previous literature [57, 94]. One day after the end of the treatments all mice were sacrificed and blood samples were obtained by using a cardiac puncture as previously described [41]. Then, peripheral blood mononuclear cells (PBMCs) were isolated as we did for humans. Blood pools from two mice were used to obtain enough PBMC mRNA concentrations.

Animals

Ikzf1 deficient mice [101] were provided by Professor Katia Georgopoulos whereas Ikzf2 deficient mice were provided by Professor Philippe Kastner [10]. Both lines, with C57BL/6 background, were backcrossed to obtain wild type ($Ik^{+/+}$:$He^{+/+}$), heterozygous for *Ikzf1* ($Ik^{\pm}$:$He^{+/+}$), heterozygous for *Ikzf2* ($Ik^{+/+}$:$He^{\pm}$) and double heterozygous mice ($Ik^{\pm}$:$He^{\pm}$). Adult males and females were used. We also used the Egr1-CreERT2 mice [7]. These mice carry a bacterial artificial chromosome (BAC) including the Egr1 gene in which the coding sequence was replaced by that of CreERT2 fusion protein. They were crossed with R26RCE mice (Gt(ROSA)26Sortm1.1(CAG-EGFP)Fsh/Mmjax, Strain 004077, The Jackson Laboratory), which harbor the R26R CAG-boosted EGFP (RCE) reporter allele with a loxP-flanked STOP cassette upstream of the enhanced green fluorescent protein (EGFP) gene to create the double heterozygous mutant Egr1-CreERT2 x R26RCE mice for the experiments related with characterization of neural populations upon treatment with human secretomes. Single intraperitoneal injections of 4-hydroxytamoxifen (4-HT; #H7904, Sigma-Aldrich Chemical Co.) 50 mg/kg were administered to induce conditional Cre-dependent recombination. The animals were housed with access to food and water ad libitum in a colony room kept at 19–22 °C and 40–60% humidity, under an inverted 12/12 h light/dark cycle (from 8 A.M. to 8 P.M.). All animal procedures were approved by local committees [Universitat de Barcelona, CEEA (136/19); Generalitat de Catalunya (DAAM 10786) following the European Communities Council Directive (86/609/EU).

Behavioral tests

Behavioral phenotyping was performed following widely and previously detailed features of appropriate mouse models of schizophrenia [70] addressing the three dimensions of the symptomatology. First, free exploration and then, evaluation of D-amphetamine-induced hyperlocomotion (D-amphetamine sulfate, 3 mg/kg; TOCRIS 2813), were both evaluated in the open field as described elsewhere [81]. Next, sociability was assessed by using the three-chamber social interaction test as previously described [81]. Finally, object recognition long-term memory was evaluated by performing the novel object recognition test (NORT) as we previously reported [6]. In all behavioral studies animals were tracked and recorded with Smart junior 3.0 software (Panlab).

Golgi staining

Fresh brain hemispheres were submerged and processed following the Golgi-Cox method as described elsewhere [28]. Two hundred microns sections were cut in 70% EtOH on a vibratome (Leica) and washed in water for 5 min. Next, they were reduced in 16% ammonia solution for 1 h before washing in water for 2 min and fixation in Na2S2O3 for 7 min. After a 2-min final wash in water, sections were mounted on superfrost coverslips, dehydrated for 3 min in 50%, then 70, 80 and 100% EtOH, incubated for 5 min in a 2:1 isopropanol:EtOH mixture, followed by 1×5 min in pure isopropanol and 2×5 min in xylol. Bright-field images of Golgi-impregnated stratum radiatum dendrites from hippocampal CA1 pyramidal neurons or from pyramidal neurons of the medial prefrontal cortex (Layer V) or from medium spiny neurons in the striatum, were captured with a Nikon DXM 1200F digital camera attached to a Nikon Eclipse E600 light microscope (×100 oil objective). Only fully impregnated neurons with their soma entirely within the thickness of the section were used. Image z-stacks were taken every 0.2 mm, at 1024×1024-pixel resolution, yielding an image with pixel dimensions of 49.25×49.25 µm. Segments of proximal dendrites were selected for the analysis of spine density. Only spines arising from the lateral surfaces of the dendrites were included in the study. Given that spine density increases as a function of the distance from the soma, reaching a plateau 45 µm away from the soma, we selected dendritic segments of basal dendrites 45 µm away from the cell body. The total number of spines was obtained using the cell counter tool in the ImageJ software.

Quantitative proteomics

Proteins from secretome media were precipitated with acetone, and pellets dissolved in 8 M Urea, 50 mM DTT. Protein quantitation was performed with the Bradford assay kit (Bio-Rad, Hercules, CA, USA). Protein extracts (20 µg) were diluted in Laemmli sample buffer and loaded into a 1,5 mm thick polyacrylamide gel with a 4% stacking gel cast over a 12.5% resolving gel. The run was stopped as soon as the front entered 3 mm into the resolving gel so that the whole proteome became concentrated in the stacking/resolving gel interface. Bands were stained with Coomassie Brilliant Blue, excised from the gel and protein enzymatic cleavage was carried out with trypsin (Promega; 1:20, w/w) at 37 °C for 16 h as previously described [87]. Purification and concentration of peptides were performed using C18 Zip Tip Solid Phase Extraction (Millipore). For LC–MS/MS, dried peptide samples were reconstituted with 2% ACN-0.1% FA (Acetonitrile-Formic acid) and quantified by NanoDropTM spectrophometer (ThermoFisher) before LC–MS/MS analysis using an EASY-1000 nanoLC system coupled to an Exploris 480 mass spectrometer (Thermo Fisher Scientific). Peptides were resolved using a C18 Aurora column (75 µm × 25 cm, 1.6 µm particles; IonOpticks) at a flow rate of 300 nl/min using a 60-min gradient (50 °C): 2% to 5% B in 1 min, 5% to 20% B in 48 min, 20% to 32% B in 12 min, and 32% to 95% B in 1 min (A = FA, 0.1%; B = 100% ACN:0.1% FA). The spray voltage was set at 1.6 kV, and the capillary temperature at 275 °C. Sample data was acquired in a data-independent mode (DIA) with a full MS scan (scan range: 400 to 900 m/z; resolution: 60,000; maximum injection time: 50 ms; normalized AGC target: 100%) and 25 periodical MS/MS segments, applying 20 Th isolation windows (0.5 Th overlap; resolution: 15,000; maximum injection time: 22 ms; normalized AGC target: 3000%). Peptides were fragmented using a normalized HCD collision energy of 30%. Data were acquired in profile and centroid mode for full MS scan and MS/MS, respectively. For data analysis of quantitative proteomics DIA data files were analyzed using Spectronaut (v 17.3, Biognosys) by directDIA analysis (dDIA). Sample raw data was first processed by the Pulsar Spectronaut search engine to generate a spectral library. Pulsar then searched MSMS spectra against Uniprot-Swissprot isoforms Homo Sapiens database. MS1/MS2 calibration and main search tolerance were set to dynamic. The maximum precursor ion charge was set to 4, and fragment selection to intensity-based. Carbamidomethyl (C) was selected as a fixed modification, and Oxidation (M), Acetyl (Protein N-term), Deamidation (N), and Gln- > pyro-Glu as variable modifications (3 maximum modifications per peptide). The enzyme was set to trypsin in a specific mode (two missed cleavages maximum). The target-decoy-based false discovery rate (FDR) filter for PSMs, peptide, and protein groups was set to 1%. Once the Pulsar search was performed, the Spectronaut DIA search engine algorithm initiated the DIA search using the default settings (Proteotypicity filter = Protein group Specific) and filtering the precursors and protein groups by a 1% Q-value. The Perseus software (version 1.6.15.0) [96] was used for statistical analysis and data visualization. Identifications from the reverse database, common contaminants and proteins only identified through a modification peptide were removed. Label-free intensities were then logarithmized (base 2) and the samples were then grouped according to the experimental design. A filter of 70% valid values at least in one group was applied to the resulting matrix followed by a logarithmic transformation (Log2). Then, data were imputated based on the normal distribution and normalized using the "Width adjustment" method. Statistical analysis was performed using "Two-sample tests" for the T-test of two selected experimental groups, based

on permutation-based FDR statistics (250 permutations; FDR 1⁄4 0.07; S0 1⁄4 0.1). The resulting matrixes were exported containing the p-value (-Log) and fold-change (Log2) columns that, after its transformation into linear scale, were filtered by $p < 0.05$ and 30% of significance and fold-change respectively.

Luminex assay

We measured a panel of 30 cytokines, chemokines and growth factors in 14 supernatant samples by Luminex using the Cytokine Human Magnetic 30-Plex Panel LHC6003M from Life Technologies™. Briefly, 25 µl of the sample were tested by applying a modification to the manufacturer's protocol by using half the volume of all reagents including the standards. This modification has been previously tested and showed no difference in assay performance compared to the original protocol and has been used in prior studies [1, 37]. Each plate included 16 serial dilutions (twofold) of a standard sample with known concentrations of each analyte and two blanks. Samples were acquired on a Luminex® 100/200 instrument and analyzed with xPONENT® software 3.1. Concentrations of analytes were obtained by interpolating the median fluorescent intensity (MFI) to a 5-parameter logistic regression curve fitted with the R package (drLumi) [82]. If the algorithm did not converge, a 4-parameter log-logistic model was fitted. Limits of quantification (LOQ) were estimated based on the 30% threshold value for the coefficient of variation (CV) of the standard curve. Molecules outside the LOQ in more than 30% of samples were excluded from the study. For all other markers, observations outside LOQ were imputed. Results were reported as pg/mL. The Luminex assay was performed in the Immune Response and Biomarkers Core Facility at ISGlobal (Barcelona, Spain).

Hippocampal primary cultures and immunocytochemistry

Hippocampal neurons were obtained from E17.5 C57Bl/6 mice. The hippocampus was dissected and mechanically dissociated with a fire-polished Pasteur pipette. Cells were seeded at a density of 50,000 onto 12 mm coverslips placed in 24-well plates. Plates were previously precoated with 0.1 mg/mL poly-D-lysine (Sigma-Aldrich Chemical Co., St. Louis, MO, USA) and neurons were cultured in Neurobasal medium (Gibco-BRL, Renfrewshire, UK) supplemented with 1% Glutamax and 2% B27 (Gibco-BRL). Cultures were maintained at 37 °C in a humidified atmosphere containing 5% CO_2. Primary neurons were fixed with 4% paraformaldehyde solution in PBS for 10 min and blocked in PBS-0.1 M glycine for 10 min. Then, cells were permeabilized in PBS-0.1% saponin 10 min, blocked with PBS-Normal Horse Serum 15% for 30 min, and incubated overnight at 4 °C in the presence of the following primary antibodies: mouse MAP2 (1:500, M1406, Sigma-Aldrich Chemical Co.) and rabbit PSD-95 (1:500, Cell Signaling, Ref: 3450S). Fluorescent secondary antibodies: AlexaFluor 488 goat anti-rabbit (1:100) and/or Cy3 goat anti-mouse (1:100; both from Jackson ImmunoResearch, West Grove, PA, USA) were incubated for 1 h at RT. Nuclei were stained with DAPI-Fluoromount (SouthernBiotech, Birmingham, AL, USA). Immunofluorescence was analyzed using a Leica Confocal SP5-II confocal microscope (Leica Microsystems CMS GmbH, Mannheim, Germany). Images were taken using an HCX PL APO lambda blue 63.0×1.40 OIL objective with a standard pinhole (1 AU), at 1024×1024-pixel resolution, 0.2 µm thick, and 5.0 digital zoom.

Tissue fixation and immunofluorescence

Mice were euthanized by cervical dislocation. Left hemispheres were removed and fixed for 72 h in 4% paraformaldehyde (PFA) in PBS. 40 µm coronal sections were obtained using a Leica vibratome (Leica VT1000S). Next, free-floating sections were washed three times in PBS, treated with NH_4Cl for 30 min, and washed again three times with PBS. Floating sections were permeabilized and blocked with PBS containing 3% Triton X-100, 0.02% Azide, 2% BSA, and 3% NGS (Ab buffer) for 1 h at RT. After three washes in PBS, brain slices were incubated overnight at 4 °C with anti-GFP (1:500, Synaptic Systems, 132006) and anti-Parvalbumin (1:1250, Swant, PV27). Sections were washed three times and incubated for 2 h at RT with fluorescent secondary antibody Alexa Fluor 488 or 647 (1:400; from Jackson Immuno Research, West Grove, PA, USA). Nuclei were stained with DAPI-Fluoromount (SouthernBiotech, Birmingham, AL, USA). Sections were analyzed using a two-photon confocal microscope (Leica SP5). To stain microglia and astrocytes in the hippocampal CA1, anti-Iba1 (1:500, Abcam, #Ab5076) and anti-GFAP (1:500, Synaptic Systems, #132006) were the antibodies employed respectively. Morphometric analysis of GFAP-positive astrocytes and Iba1-positive microglia were performed as described elsewhere [81].

Imaging analysis

To evaluate neuronal morphology by using the Sholl analysis we employed the protocol described elsewhere [18]. For the experiments evaluating PSD-95-positive puncta in primary cultures, we followed the protocol previously described [28]. For quantification of the number of activated neural ensembles and the number of parvalbumin-positive cells in the hippocampal CA1 from Egr1-CreERT2 x R26RCE mice, we used the procedure previously reported by our group [80].

3D Cell culture preparation

Tridimensional neurospheres networks were developed as previously described [72]. Briefly, E18 C57BL/6JOlaHsd pregnant mice were euthanized by cervical dislocation. Hippocampus were dissected in Neurobasal (Gibco) ice-cold media and incubated in 0.25% Trypsin–EDTA (Gibco) at 37 °C for 20 min, followed by 5 min DNAse I (1 µg/ml; Sigma-Aldrich Chemical Co.) incubation at room temperature. Mechanical dissociation of the dissected hippocampus was performed by repeated pipetting with a fire-polished glass Pasteur pipette until a homogenous cell suspension was obtained. Cell viability was determined by Trypan Blue exclusion assay. The cell solution was then centrifuged at 150 g for 10 min, and the supernatant was removed. The resulting cell pellet was resuspended in the culture media containing Neurobasal media, 2% B27, 1% N2, 0.5 mM Glutamate, and 1% Penicillin/Streptomycin (Gibco). Cells were infected with AAV7m8.Syn.GCaMP6s.WPRE.SV40 virus (Unitat de Producció de Vectors, Universitat Autonoma Barcelona) for neuronal GCaMP6s calcium sensor expression. The viral infection was made at 1:1000 dilution at the single-cell suspension stage, just before seeding. For neurospheres network cultures, 5.5×10^4 cells were seeded in poly-dimethylsiloxane (PDMS) customized molds containing an 18 mm^2 square well. PDMS molds were fabricated in UV resin 3D printed cast (Formlab 3 + laser 3D printer) and polymerized overnight at 90 °C. Neurospheres cultures were incubated in culture media at 37 °C and 5% CO_2. Imaging experiments were performed using a wide-field fluorescence microscope (Inverted microscope Zeiss Axio Observer Z1) and ZEN software (Zeiss) was used for image acquisition. Time-lapse videos were recorded at 25 Hz for 5 min at 37 °C and 5% CO_2 in culture media (Neurobasal media, 2% B27, 0.5 mM Glutamate, and 1% Penicillin/Streptomycin (Gibco)). Videos were acquired at DIV28. All computations and visualizations were done using the standard Python-based ecosystems for scientific computing and data visualization (NumPy, SciPy, Seaborn, SciKitLearn, Matplotlib). Statistical significance was plotted using the stat annotations package (https://github.com/trevismd/statannotations). Video data was extracted from.czi files. For neurosphere segmentation was done using the Otsu thresholding technique. A time series of mean intensity values of each neurosphere was extracted. The signal was denoised using a Butterworth filter. After normalization, peaks were detected (prominence (1-mean)/3, height 0.5) and the signal was binarized. Neurospheres without any detected activity were discarded from the subsequent analysis. From the binarized signal the following parameters were computed: mean activity rate, mean peak duration, and average pairwise Pearson correlation of neurospheres. Statistical significance between different conditions was determined at DIV28 by one-way ANOVA and Dunnett's as *post-hoc* test. A subset of neurospheres were fixed and stained against Tuj1 (1:1000, #T8660; Sigma).

Mini-osmotic pumps implantation

Mice were deeply anesthetized with isoflurane (2% induction, 1.5% maintenance) and 2% oxygen and placed in a stereotaxic apparatus for osmotic minipump (model 1004; Alzet, Palo Alto, CA, USA) implantation. A brain infusion kit (#0008663) was also used to deliver into the lateral (left) ventricle (0.1 mm posterior to bregma, ± 0.8 mm lateral to the midline, and − 2.5 mm ventral to the parenchyma surface) 0.11 µl per hour of supernatants obtained from cultured peripheral blood mononuclear cells/PBMC at a protein concentration of 0,2064 µg/µl. Cannulas were fixed on the skull with Loctite 454 (from Alzet). Minipumps, previously equilibrated overnight at 37 °C in PBS, were implanted subcutaneously in the back of the animal. After recovery, the mice were isolated to prevent detachment of the cannulas.

Statistics

All data are expressed as mean ± SEM. Statistical analysis was performed using the unpaired two-sided Student's t test (95% confidence), one-way ANOVA with Tukey's as post hoc tests, or two-way ANOVA with Bonferroni's post hoc test as appropriate and indicated in the figure legends. Values of $p < 0.05$ were considered statistically significant. All experiments in this study were blinded and randomized. All mice bred for the experiments were used for preplanned experiments and randomized to experimental groups. Visibly sick animals were excluded before data collection and analysis. Data were collected, processed, and analyzed randomly. The experimental design and handling of mice were identical across experiments. Littermates were used as controls with multiple litters (3–5) examined per experiment.

Results

IKZF1 and *IKZF2* mRNA expression levels are specifically downregulated in peripheral blood mononuclear cells in patients with schizophrenia

Since we have previously reported that mice full knockout for *Ikzf1* or *Ikzf2* could develop brain-related deficiencies [5, 29, 60, 61], we first aimed to assess *IKZF1* and *IKZF2* mRNA levels by RT-qPCR in different brain regions strongly implicated in the pathophysiology of schizophrenia, namely the hippocampus, dorsolateral prefrontal cortex (DLPFC), and putamen. We evaluated such mRNA levels in post-mortem brain samples from patients with schizophrenia and control patients (Suppl Table 1). We did not detect changes in *IKZF1* and *IKZF2*

mRNA levels in either, the hippocampus (Fig. 1a, b) or the DLPFC (Fig. 1c, d) or putamen (Fig. 1e, f) when comparing samples from schizophrenia patients with samples from control subjects. The same results were observed when protein levels were evaluated by western blot (Suppl. Figure 1). We next hypothesized that, since *IKZF1* and *IKZF2* in adult mammals are both more enriched in circulating immune (lymphocytes) cells than in neural tissues [44] (see also in *The Human Protein Atlas*), it would be conceivable that potential changes could be easier to be detected there rather than in the brain. Thus, we isolated peripheral blood mononuclear cells (PBMCs), which are mostly ~ 70–90% lymphocytes [86], from controls and patients with schizophrenia (Suppl Table 2). A descriptive evaluation of these PBMCs showed no differences in terms of cell density for either, neutrophils or

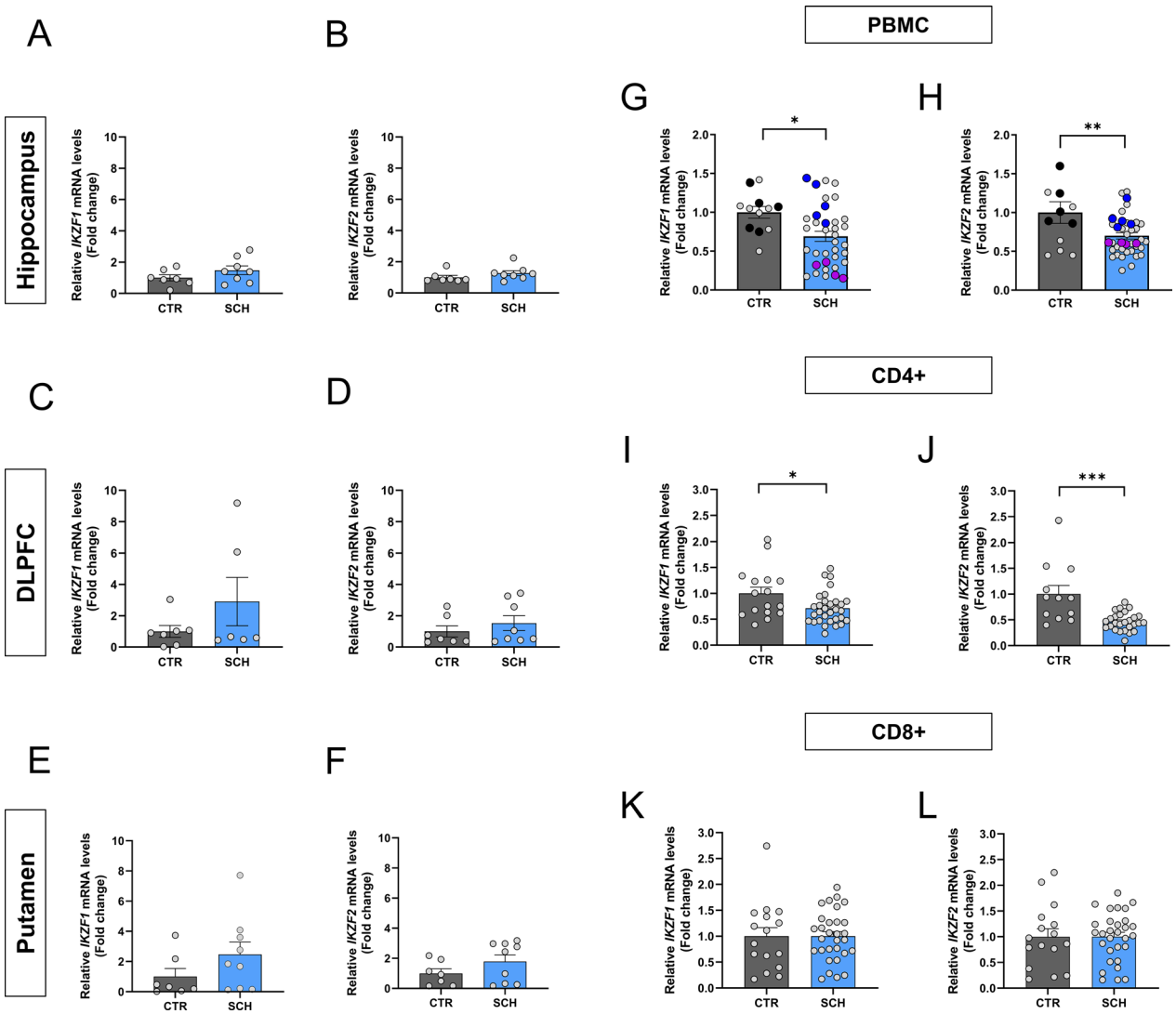

Fig. 1 *IKZF1* and *IKZF2* mRNA levels in the brain and circulating immune cells of patients with schizophrenia. Determination of *IKZF1* and *IKZF2* mRNA levels in different brain regions. Results from RT-qPCR of total *IKZF1* and *IKZF2* mRNA levels in different brain regions namely hippocampus (**a** and **b** respectively), dorso-lateral prefrontal cortex (DLPFC, **c** and **d** respectively) and putamen (**e** and **f** respectively) from patients with schizophrenia (SCH) or matched controls (CTR). Demographics of the samples are displayed in supplementary Table 1. Results from RT-qPCR of total (**g**) *IKZF1* and (**h**) *IKZF2* mRNA levels in peripheral blood mononuclear cells (PBMCs) isolated from patients with schizophrenia (SCH) or matched controls (CTR). Highlighted black, blue and violet dots are the samples selected for the subgroups used in Fig. 4 onwards (CTR, SCH^{Ik+He+} and SCH^{Ik-He-} groups respectively). (**i**) Results from RT-qPCR of total *IKZF1* and (**j**) *IKZF2* mRNA levels in CD4 + cells isolated from PBMCs in **i**-**j**. Results from RT-qPCR of total (**k**) *IKZF1* and (**l**) *IKZF2* mRNA levels in CD8 + cells isolated from PBMCs in **i**-**j**. Demographics of the samples are displayed in supplementary Table 2. Data are means ± SEM and they were analyzed using the two-tailed Student t-test. *$p < 0.05$, **$p < 0.01$ and ***$p < 0.001$ vs CTR

lymphocytes or monocytes when comparing control subjects with patients with schizophrenia (Suppl Table 3). We then extracted their mRNA and evaluated *IKZF1* and *IKZF2* mRNA levels. Interestingly, we detected that *IKZF1* (Fig. 1g) and *IKZF2* (Fig. 1h) were both significantly downregulated in PBMCs mRNA from patients with schizophrenia compared to matched controls. As we did for brain regions, we also confirmed these results at protein levels for IKZF1 but not for IKZF2 (Suppl. Figure 1 and Suppl. Table 4). We then looked at isolated CD4 + and CD8 + cells from the same PBMCs. We found that *IKZF1* (Fig. 1i) and *IKZF2* (Fig. 1j) mRNA levels were both downregulated in CD4 + cells. In contrast, *IKZF1* (Fig. 1k) and *IKZF2* (Fig. 1l) mRNA levels were normal in CD8 + cells. Next, to rule out the possibility of unspecific effects mediated by the medications on these changes we decided to sub-chronically treat wild type mice for 7 days with the two most common administered antipsychotics in our cohort of patients; paliperidone and clozapine. We found that *Ikzf1* and *Ikzf2* mRNA levels in mouse PBMCs were not affected by such treatments (Suppl Fig. 2). To further ensure this result we repeated the experiment with a more chronic treatment (28 days) focusing with the most employed antipsychotic in all our cohorts of patients, clozapine. Again, no changes in either *Ikzf1* or *Ikzf2* mRNA levels in mouse PBMCs were found (Suppl. Figure 2). Altogether, these results indicate that the double reduction of *IKZF1* and *IKZF2* mRNA levels in PBMCs is localized in CD4 + cells. These alterations could play a role in the dysfunctions described for this cell type in the context of schizophrenia [15].

Mimicking the double *Ikzf1* and *Ikzf2* downregulation in mice results in a myriad of several schizophrenia-like disturbances

Although many different expressed genes (DEGs) and proteins (DEPs) have been identified in patients with schizophrenia, most of them have not been yet characterized or their role in the pathophysiology of the disease remain, at least, controversial [77, 83, 91]. Therefore, we aimed to characterize the relevance of this double reduction by mimicking it in mice. To do so we crossed heterozygous mice for *Ikzf1* ($Ik^{\pm}$:$He^{+/+}$, [61] with heterozygous mice for *Ikzf2* ($Ik^{+/+}$:$He^{\pm}$, [60]) to generate double mutant mice with a double reduction of both, *Ikzf1* and *Ikzf2* ($Ik^{\pm}$:$He^{\pm}$, Fig. 2a). Since both, adult (4–5 months of age) $Ik^{\pm}$:$He^{+/+}$ and $Ik^{+/+}$:$He^{\pm}$ mice displayed only some phenotypes compared to $Ik^{+/+}$:$He^{+/+}$ mice (Suppl. Figure 3), henceforth we focused on the $Ik^{+/+}$:$He^{+/+}$ and $Ik^{\pm}$:$He^{\pm}$ genotypes (a.k.a. Wild type mice and double mutant mice) only. First, the appearance and body weight (Suppl. Figure 4) were indistinguishable between the two groups, thus suggesting a normal health state in male and female $Ik^{\pm}$:$He^{\pm}$ mice. Then, to evaluate the potential schizophrenia-like phenotypes in our mutant mice, we performed a broad behavioral characterization aimed to evaluate positive, negative and cognitive symptomatology as previously established [70]. Regarding the positive-like phenotypes, we first observed that $Ik^{\pm}$:$He^{\pm}$ females (Fig. 2b) and $Ik^{\pm}$:$He^{\pm}$ males (Fig. 2c) displayed increased basal locomotion/agitation in the open field paradigm when compared with their matched $Ik^{+/+}$:$He^{+/+}$ controls. Furthermore, both, $Ik^{\pm}$:$He^{\pm}$ males (Fig. 2d) and females (Fig. 2e) showed an increased sensitivity to the D-Amphetamine in an open field arena. Regarding the negative-like phenotypes, we observed that in the three-chamber social interaction test there was a consistent alteration in sociability showed by both $Ik^{\pm}$:$He^{\pm}$ males (Fig. 2f) and females (Fig. 2g) compared with their matched controls. Finally, long-term declarative memory was also assessed by subjecting the groups of mice to the novel object recognition test (NORT). First, females $Ik^{\pm}$:$He^{\pm}$ were uncapable to recognize the new object with respect the old one when compared to $Ik^{+/+}$:$He^{+/+}$ controls (Fig. 2h). Similarly, $Ik^{+/+}$:$He^{+/+}$ males showed preference for the new object whereas $Ik^{\pm}$:$He^{\pm}$

(See figure on next page.)

Fig. 2 Generation and characterization of the $Ik^{\pm}$:$He^{\pm}$ double mutant mice. **a** Schematic representation of the adult mutant mice generated and used. $Ik^{\pm}$ and $He^{\pm}$ mice were crossed to generate the four genotypes; $Ik^{+/+}$:$He^{+/+}$, $Ik^{+/+}$:$He^{\pm}$, $Ik^{\pm}$:$He^{+/+}$ and $Ik^{\pm}$:$He^{\pm}$. Since the behavioral phenotype in $Ik^{+/+}$:$He^{\pm}$ and $Ik^{\pm}$:$He^{+/+}$ groups of mice were punctual compared to that in $Ik^{+/+}$:$He^{+/+}$ mice (Suppl. Figure 3), we focused on the controls $Ik^{+/+}$:$He^{+/+}$ and the double mutant $Ik^{\pm}$:$He^{\pm}$ mice. Basal locomotor activity was evaluated in the two groups of mice separated into (**b**) females (Genotype effect: $F_{(1, 495)} = 22{,}58$, $p < 0.0001$) and (**c**) males (Genotype effect: $F_{(1, 538)} = 9{,}518$, $p = 0.0021$) in a 15 min testing session of free exploration in an open field. Induced agitation and sensitivity to the psychostimulant D-amphetamine was measured in a 45 min testing session upon injection of 5 mg/Kg of D-amphetamine in (**d**) female (Genotype effect: $F_{(49, 1450)} = 20{,}37$, $p < 0.0001$) and (**e**) male (Genotype effect: $F_{(48, 1666)} = 21{,}28$, $p < 0.0001$) mice from both groups. Sociability was evaluated in the three-chamber social interaction test (TCSIT). Mice from the two groups were subjected to the TCSIT and data were depicted for (**f**) females (Social preference effect: $F_{(1, 60)} = 8{,}456$, $p = 0.0051$) and (**g**) males (Social preference effect: $F_{(1, 64)} = 19{,}36$, $p < 0.0001$). Recognition memory was evaluated in the novel object recognition test (NORT) 24 h after a training session. Mice from two groups were subjected to the NORT and data were depicted for (**h**) females (NORT preference effect: $F_{(1, 54)} = 5{,}415$, $p = 0.0237$) and (**i**) males (NORT preference effect: $F_{(1, 66)} = 18{,}35$, $p < 0.0001$). Data are means ± SEM and they were analyzed using the two-way ANOVA. *$p < 0.05$, ***$p < 0.001$ vs $Ik^{+/+}$:$He^{+/+}$ mice in **b**, **d** and **e**. In **f**, **g**, **h,** and **i** data were analyzed using the two-way ANOVA with Bonferroni's post hoc test; **$p < 0.01$ and ***$p < 0.001$ vs time exploring the stranger or the new object

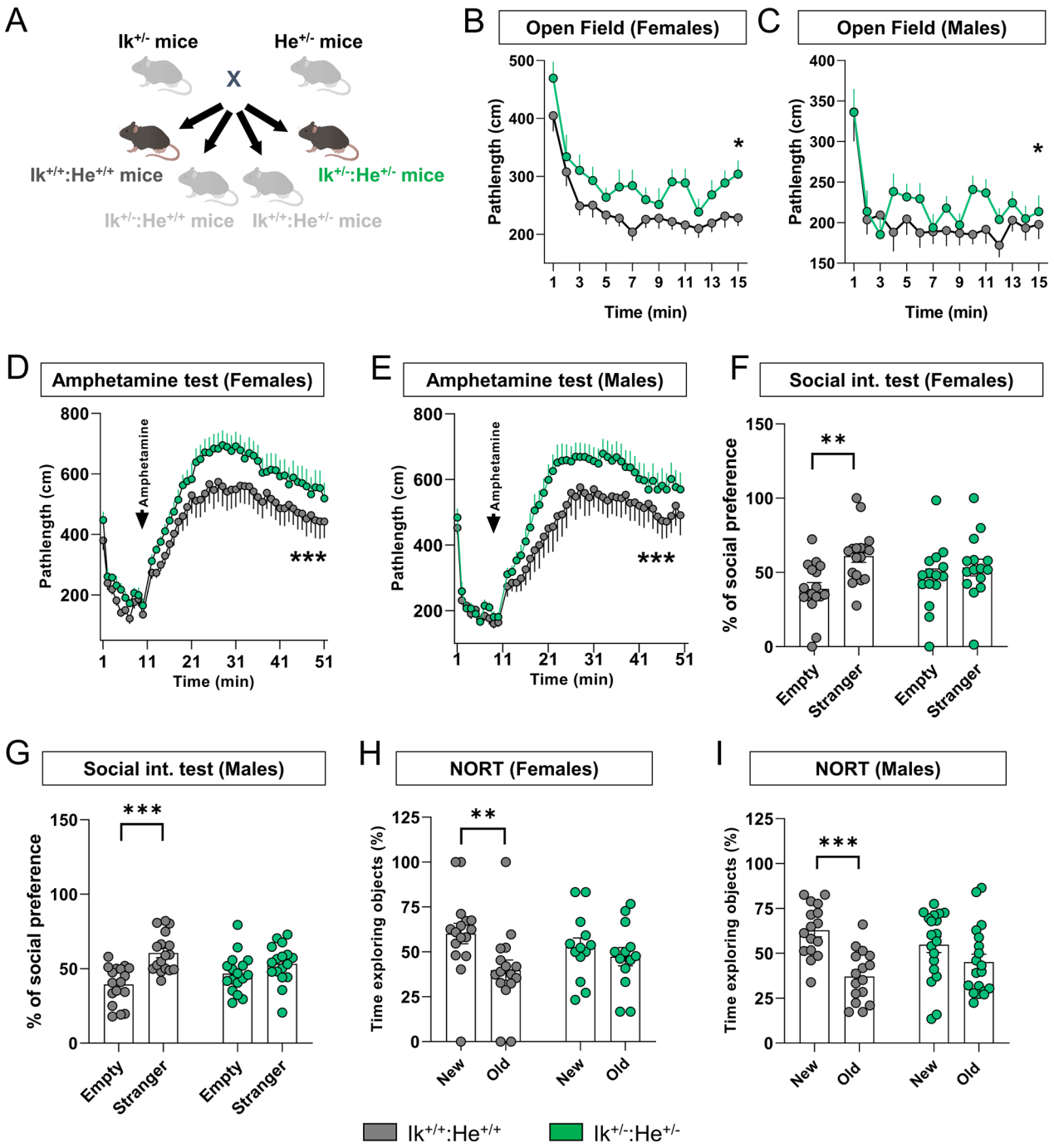

Fig. 2 (See legend on previous page.)

males did not (Fig. 2i), suggesting the presence of detectable cognitive deficits in both Ik$^{\pm}$:He$^{\pm}$ males and females.

To further assess associated schizophrenia-like phenotypes such as dendritic spine loss in several brain regions as described elsewhere in post-mortem samples from patients [30], we quantified spine density in hippocampal CA1 pyramidal neurons, in Medium Spiny Neurons (MSNs) of the dorsal striatum and in pyramidal neurons of the layer V in the medial pre-frontal cortex (mPFC) of Ik$^{+/+}$:He$^{+/+}$ and Ik$^{\pm}$:He$^{\pm}$ mice. First, we identified a significant reduction of dendritic spine density in the MSNs of both, Ik$^{\pm}$:He$^{\pm}$ males (Fig. 3a) and Ik$^{\pm}$:He$^{\pm}$ females (Fig. 3b) compared with their respective Ik$^{+/+}$:He$^{+/+}$ controls. In contrast, alterations in spine density of the

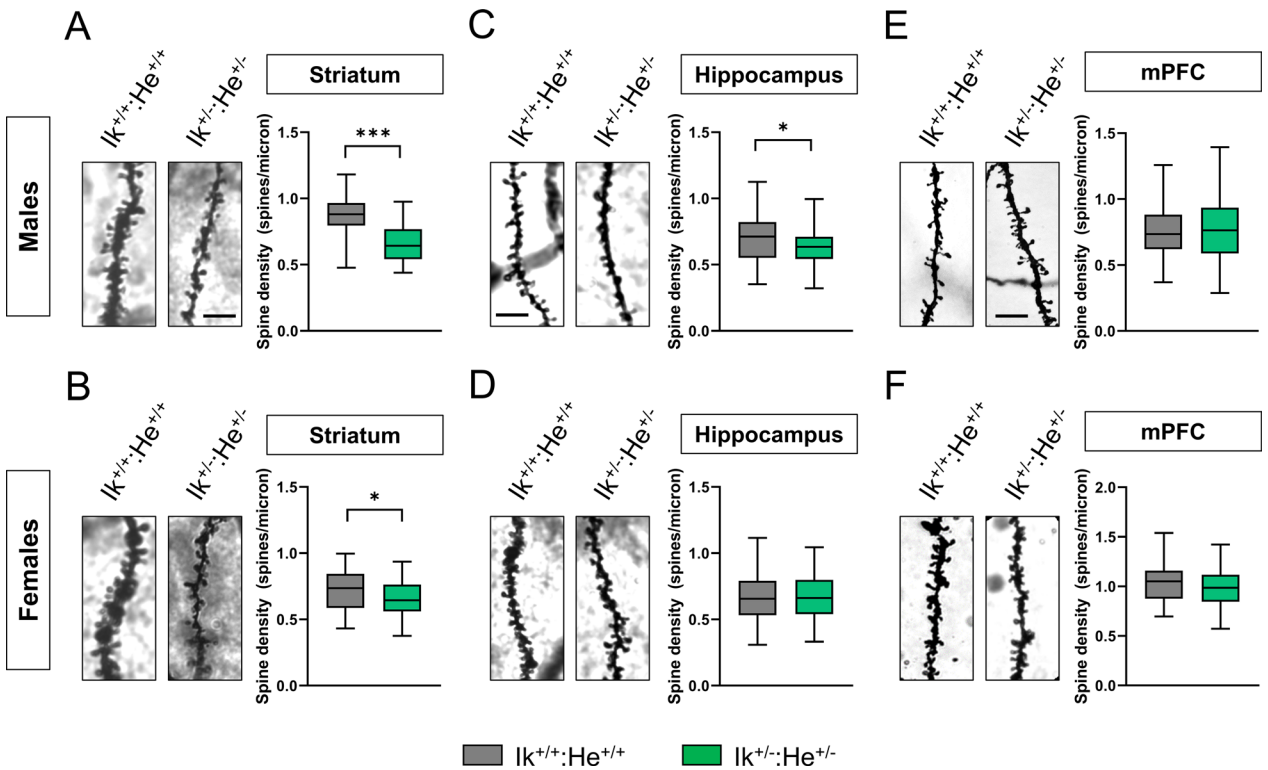

Fig. 3 Characterization of structural synaptic plasticity in the Ik$^{\pm}$:He$^{\pm}$ mice. **a**, **b** Representative images (left panels) and quantification (right panels) of spine density in dendrites from medium spiny neurons (MSNs) of the dorsal striatum labeled with Golgi staining. Images were obtained in a bright-field microscope in adult (**a**) male and (**b**) female Ik$^{+/+}$:He$^{+/+}$ and Ik$^{\pm}$:He$^{\pm}$ mice. Scale bar, 5 µm. **c**, **d** Representative images (left panels) and quantification (right panels) of spine density in secondary apical dendrites from pyramidal neurons of the hippocampal CA1 labeled with Golgi staining. Images were obtained in adult (**c**) male and (**d**) female Ik$^{+/+}$:He$^{+/+}$ and Ik$^{\pm}$:He$^{\pm}$ mice. Scale bar, 5 µm. **e**, **f** Representative images (left panels) and quantification (right panels) of spine density in dendrites from pyramidal neurons of layer V in the frontal cortex labeled with Golgi staining. Images were obtained in adult (**e**) male and (**f**) female Ik$^{+/+}$:He$^{+/+}$ and Ik$^{\pm}$:He$^{\pm}$ mice. Scale bar, 5 µm. Data are means ± SEM and they were analyzed using the two-tailed Student t-test. *p < 0.05, ***p < 0.01 vs Ik$^{+/+}$:He$^{+/+}$ mice. In **a**, n = 50–54 dendrites/genotype (from 7 mice/genotype). In **b**, n = 54–66 dendrites/genotype (from 7 mice/genotype). In **c**, n = 62–65 dendrites/genotype (from 7 mice/genotype). In **d**, n = 60–68 dendrites/genotype (from 7 mice/genotype). In **e**, n = 89–55 dendrites/genotype (from 7 mice/genotype). In **f**, n = 43–47 dendrites/genotype (from 7 mice/genotype). Scale bar in **a**, 5 µm

CA1 pyramidal cells was only observed in Ik$^{\pm}$:He$^{\pm}$ males (Fig. 3c), but not in Ik$^{\pm}$:He$^{\pm}$ females (Fig. 3d). Finally, regarding to spine density in pyramidal neurons of the mPFC, no changes were observed in any condition (Fig. 3e-f). In conclusion, our newly generated double Ik$^{\pm}$:He$^{\pm}$ mutant mice mimic several features (behavioral and histological) in mice that are also observed in patients with schizophrenia and models.

IKZF1 and *IKZF2* mRNA levels in PBMC regulate the molecular profile of their secretome in patients with schizophrenia

Upon the observation that Ik$^{\pm}$:He$^{\pm}$ mice mimicked schizophrenia-like features, we next aimed to study which is the underlying molecular bridge between the circulating immune system and central nervous system that induces these phenotypes. We hypothesized that altered levels of *IKZF1* and *IKZF2* could impair the transcriptional activity of secreted molecules (secretome) by these circulating immune cells such as cytokines, chemokines, growth factors and other molecules. These impaired secretomes could, in turn, impair neural networks involved with the development of schizophrenia. To address these questions, we opted to use a more translational approach (Suppl. Figure 5a). From patients with schizophrenia studied in Fig. 1g, h, we generated two sub-groups of patients; the first with normal levels of *IKZF1* and *IKZF2* (SCH$^{Ik+:He+}$ group) in PBMC and the second with a double down-regulation of both, *IKZF1* (> 40%) and *IKZF2* (> 40%) in PBMC (SCH$^{Ik-:He-}$ group) compared to control (CTR) patients (Suppl. Figure 5b-c). All groups were matched in terms of number (n = 4–5/group), age (Suppl. Figure 5d), sex, and the PANSS general score (Suppl. Table 5). Also, the number of circulating lymphocytes, neutrophils, platelets, and monocytes were indistinguishable between SCH$^{Ik+:He+}$

and $SCH^{Ik-:He-}$ groups (Suppl. Figure 5e-h). Additionally, based on this criterion of > 40% of reduction, it is worth mentioning the proportion of patients for each condition (Suppl Fig. 2); 6 of 35 patients displayed a double downregulation of both, *IKZF1* and *IKZF2* mRNA levels. 6 of 35 patients showed reduction only in *IKZF1* mRNA levels. Finally, 4 of 35 patients showed reduction only in *IKFZ2* mRNA levels. We then obtained and cultured PBMC from all selected subjects and obtained their supernatants (a.k.a. secretomes; Suppl. Figure 5a) containing the secretome of such cells. We first performed a protein expression screening in these secretomes using a mass spectrometry approach. A principal component analysis (PCA) revealed that the two groups of patients with schizophrenia, $SCH^{Ik+:He+}$ and $SCH^{Ik-:He-}$, were different with respect to the CTR group (Fig. 4a). However, PCA indicated that $SCH^{Ik+:He+}$ and $SCH^{Ik-:He-}$ groups were slightly different between each other (Fig. 4a). Venn diagram representation indicated that 17 and 13 proteins were specifically altered in the $SCH^{Ik+:He+}$ and $SCH^{Ik-:He-}$ groups respectively compared to the CTR group. Also, only changes in 9 proteins were observed to be shared by both $SCH^{Ik+:He+}$ and $SCH^{Ik-:He-}$ groups when compared to CTR subjects (Fig. 4b, c). Proteins changing in this same sense included TUBA8, PFN1, TUBB, and DEFA1 (Fig. 4c, d). In contrast, specific altered proteins in the $SCH^{Ik+:He+}$ group comprised ACTB, COTL1, FLNA, and PRTN3. On the other hand specific altered proteins in the $SCH^{Ik-:He-}$ group involved ACTR3, SH3BGRL, LUZP1, CFL1, CCL5 (RANTES), C1RL and RHOC. To further complement these results from mass spectrometry we also performed a Luminex-based screen of several cytokines and chemokines in the supernatants from the three groups. Results indicated that some proteins were downregulated only in the $SCH^{Ik-:He-}$ group compared to the CTR group such as GMSF and IL-4 (Fig. 4f) or MIP1A (Fig. 4g). Oppositely, CXCL10 was upregulated only in the $SCH^{Ik-:He-}$ group compared to the CTR group (Fig. 4h). Finally, G-CSF and IL-10 were indistinguishable between groups (Fig. 4i). In summary, secretomes from $SCH^{Ik+:He+}$ and $SCH^{Ik-:He-}$ groups were significantly different between them and also compared to CTR secretomes.

IKZF1 and *IKZF2* mRNA levels in PBMCs from patients with schizophrenia modulate neuronal structural plasticity in primary mouse hippocampal neurons

We observed that the secretomes of both, $SCH^{Ik+:He+}$ and $SCH^{Ik-:He-}$ groups, displayed different molecular profiles between each other and also compared to CTR subjects. Next, we aimed to evaluate whether such changes could exert some impact on neuronal functions. To do so, we first set up the safety of using such secretomes from patients in mouse neuronal cultures. We first pooled the secretomes for each group. All three pools (CTR, $SCH^{Ik+:He+}$, and $SCH^{Ik-:He-}$) had a protein concentration of 2,064 µg/µl. We then added two different dilutions, 1:1 and 1:10 from the CTR secretome pool to mouse hippocampal primary neurons at day in vitro 7 (DIV7, Fig. 5a). We also used two additional controls in this experiment, namely a naïve hippocampal primary culture without any treatment and a culture only treated with PBMC media X-Vivo (as a vehicle). We observed that 24 h after treatments, the dilution 1:1 induced neuronal degeneration per se whereas the dilution 1:10 did not affect neuronal morphology as compared with the two other controls (Fig. 5b and d). Thus, we used the 1:10 concentration henceforth for the ulterior experiments using the three secretome pools due to its safety for neuronal viability. Next, we evaluated the effect of these

(See figure on next page.)

Fig. 4 Molecular profile of PBMC secretomes from stratified patients with schizophrenia. From our results in Fig. 1g, h, we selected and stratified patients as follows: Patients with schizophrenia but with unaltered mRNA levels in PBMC of both, *IKZF1* and *IKZF2* respect to CTR subjects ($SCH^{Ik+:He+}$ group; n = 5) and patients with a double reduction (≥ 40%) of *IKZF1* and *IKZF2* mRNA levels in PBMCs ($SCH^{Ik-:He-}$ group; n = 4). These stratified patients were matched to control subjects with normal *IKZF1* and *IKZF2* mRNA levels (CTR group; n = 5). From these stratified patients, supernatants of cultured PBMC were collected and subjected to Mass Spectrometry. **a** Principal component analysis (PCA) for proteomics data from PBMC supernatants. The PCA plot represents the 14 subjects from the three subgroups (CTR in grey, $SCH^{Ik+:He+}$ in blue, and $SCH^{Ik-:He-}$ in violet) that indicates subtle proteomics profile differences between such supernatants. **b** Venn diagram showing the total number of proteins differentially expressed or DEPs in each of the SCH subgroups. The common DEPs (9) comparing both groups ($SCH^{Ik+:He+}$ and $SCH^{Ik-:He-}$) with respect to the CTR group, the specific DEPs (17, blue) comparing $SCH^{Ik+:He+}$ with CTR, and the specific DEPs (13, violet) comparing $SCH^{Ik-:He-}$ with CTR are depicted. **c** Table showing the specific down-regulated (green) and up-regulated (red) DEPs in each comparison extracted from **b**. **d** Volcano plot depicting DEPs when comparing supernatants from the CTR and $SCH^{Ik+:He+}$ groups. Dashed horizontal line shows the p values cutoff, and the two vertical dashed lines indicate down/up regulated proteins. Red points indicate significantly DEPs. Dark points indicate non-significant DEPs. **e** Volcano plot depicting DEPs when comparing supernatants from the CTR and $SCH^{Ik-:He-}$ groups as we did for **d**. Analyte array measured by a Luminex assay depicting the levels in pg/ml of (**f**) FGF, IL-1B, IL-13, IL-12, IL-17, GMCSF, IL-15, HGF, VEGF, IFNg, IFNa, TNFa, IL-17, IL-2R, MIG, IL-4 and (**g**) MIP1A, MIP1B, IL-1RA, IL-8 and (**h**) Eotaxin, CXCL10 and (**i**) G-CSF and IL-10. The analytes are depicted in four (**f**–**i**) different graphs due to their huge variability in terms of the range of concentrations. Data are means ± SEM and they were analyzed using the one-way ANOVA and the Dunnet's post hoc in **f**–**i**. *p < 0.05 vs CTR group

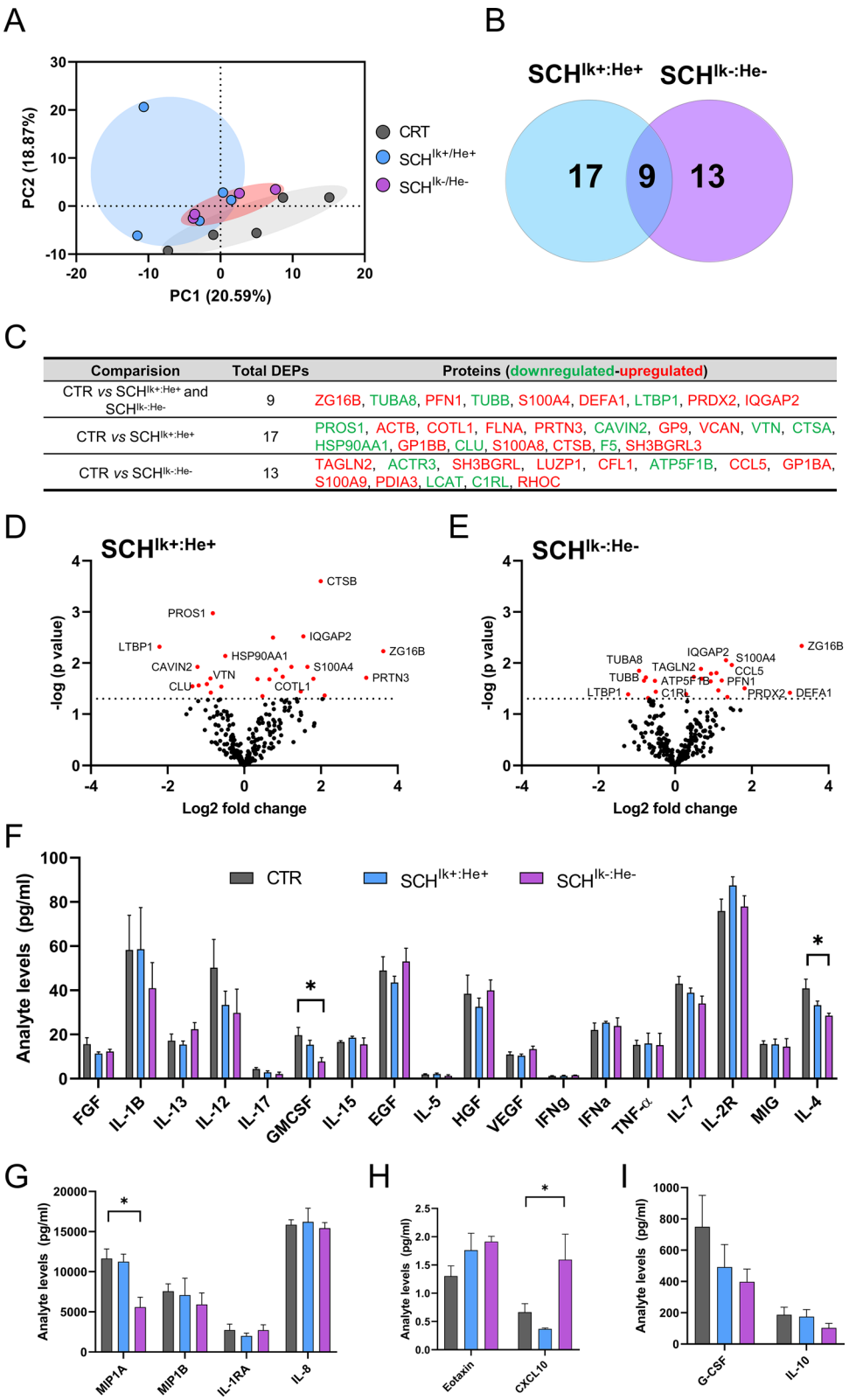

Comparision	Total DEPs	Proteins (downregulated-upregulated)
CTR *vs* SCH$^{lk+:He+}$ and SCH$^{lk-:He-}$	9	ZG16B, TUBA8, PFN1, TUBB, S100A4, DEFA1, LTBP1, PRDX2, IQGAP2
CTR *vs* SCH$^{lk+:He+}$	17	PROS1, ACTB, COTL1, FLNA, PRTN3, CAVIN2, GP9, VCAN, VTN, CTSA, HSP90AA1, GP1BB, CLU, S100A8, CTSB, F5, SH3BGRL3
CTR *vs* SCH$^{lk-:He-}$	13	TAGLN2, ACTR3, SH3BGRL, LUZP1, CFL1, ATP5F1B, CCL5, GP1BA, S100A9, PDIA3, LCAT, C1RL, RHOC

Fig. 4 (See legend on previous page.)

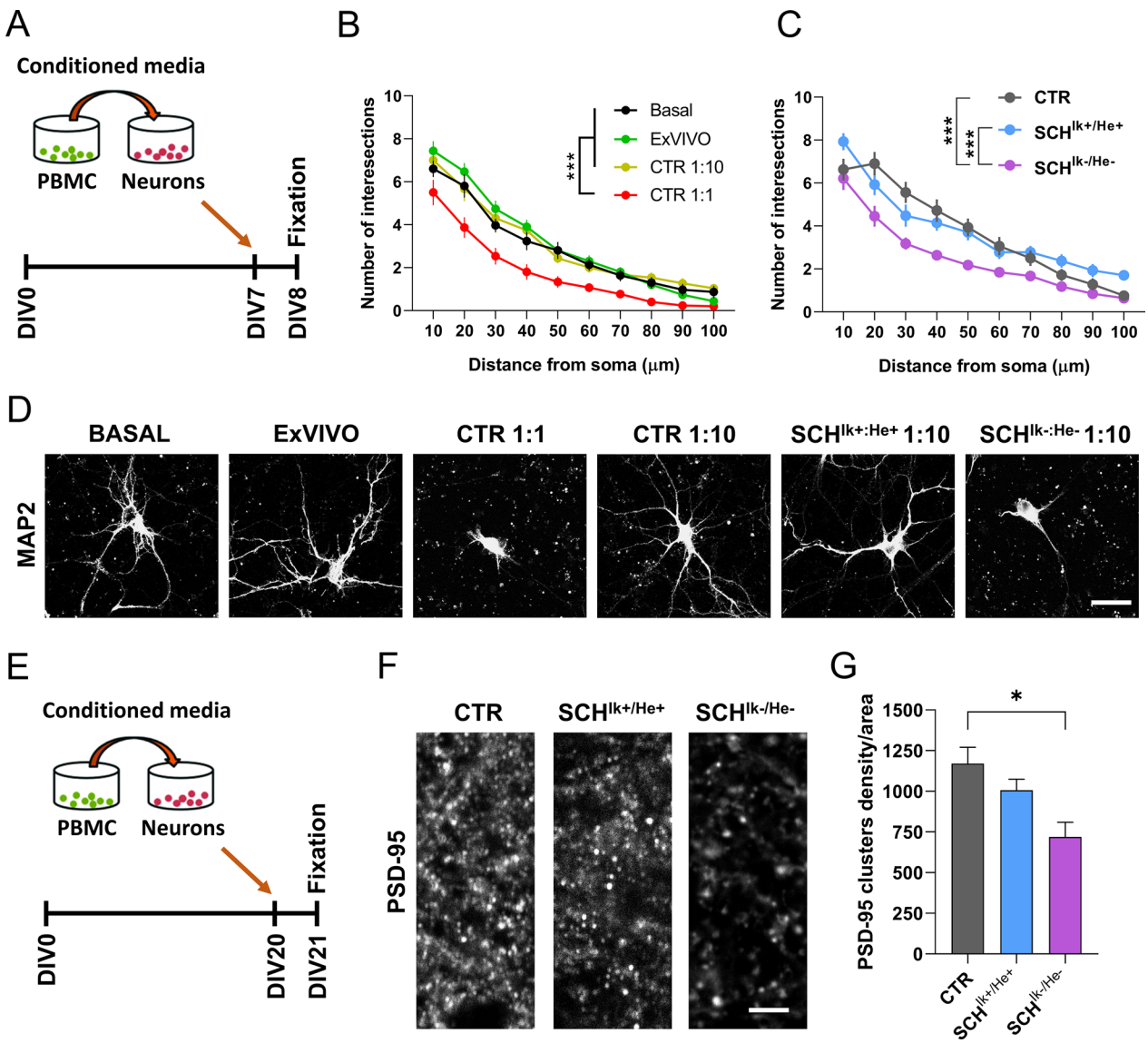

Fig. 5 Effects of CTR, SCH$^{lk+:He+}$ and SCH$^{lk-:He-}$ supernatants in neuronal structural plasticity. **a** The experimental design is depicted. Supernatants (a.k.a. conditioned media) from cultured PBMC were added to primary hippocampal neurons at DIV7 and 24 h later, their dendritic morphology was assessed by using the Sholl analysis. **b** and **d** Different concentrations (1:1 and 1:10 supernatants from the CTR pool) and controls (X-Vivo media and naïve primary neurons) were employed (Group effect: $F_{(3, 1166)} = 147{,}1$, $p < 0.0001$). The 1:10 concentration was selected as the one to be used from **c** onwards because of its safety when compared with Basal and X-Vivo control conditions (**b** and **d**). **c** and **d** Effects of CTR, SCH$^{lk+:He+}$ and SCH$^{lk-:He-}$ supernatants on neuronal branching in primary hippocampal neurons using the selected (1:10) dose (Group effect: $F_{(2, 890)} = 40{,}97$, $p < 0.0001$). In **b**-**d** MAP2 staining was employed. **e** The experimental design to evaluate synaptic changes is depicted. Supernatants (conditioned media) from cultured PBMC were added to primary hippocampal neurons at DIV20 and 24 h later (**f**) the density of PSD-95 positive puncta per area was assessed in the three groups. **g** Quantification of PSD-95-positive puncta/area from **f** ($F_{(2, 9)} = 6{,}905$, $p = 0.0152$). Data are mean ± SEM. In **b** (n = 30 neurons/group) and **c** (n = 27–33 neurons/group) the two-way ANOVA was applied and Tukey's multiple comparisons test was used as a post hoc. In **g** (n = 4 cultures/group) one-way ANOVA was applied, and Dunnett's multiple comparisons test was used as a post hoc. Scale bar in **d**, 30 μm. Scale bar in **f**, 5 μm

secretomes in neuronal branching by treating neurons at DIV7. While CTR and SCH$^{lk+:He+}$ secretomes did not induce significant changes on neuronal morphology, the SCH$^{lk-:He-}$ secretome induced a substantial reduction in the neuronal dendritic complexity (Fig. 5c, d). To further deepen on these effects, we then repeated the experiment but adding the secretomes from the three groups (CTR, SCH$^{lk+:He+}$ and SCH$^{lk-:He-}$) to primary hippocampal neuronal cultures at DIV20 (Fig. 5e). Then, 24 h later we quantified the number of PSD-95-positive clusters

(as an excitatory post-synaptic marker) in these cultures. We observed a significant reduction of PSD-95-positive clusters in primary cultures treated with the $SCH^{Ik-:He-}$ secretome but not in primary cultures treated with the $SCH^{Ik+:He+}$ secretomes compared with the CTR group (Fig. 5f, g). We concluded that the different molecular profile displayed by the $SCH^{Ik-:He-}$ PBMC secretome was probably the responsible for these specific effects on structural synaptic plasticity.

The PBMCs secretome of patients with schizophrenia modulate neuronal dynamics: role of *IKZF1* and *IKZF2*

Our previous results indicated that PBMC secretomes from patients with schizophrenia could play a role in structural synaptic plasticity, probably via modulation of synaptic components. To further explore this possibility, we benefit from a new approach called Modular Neuronal Network (MoNNets, [72]) designed to identify neural patterns (based on GcAMP6s-dependent calcium activity) in primary neurons resembling those observed in schizophrenia (Fig. 6a). Thus, MoNNets were generated, transduced with GcAMP6s and treated with CTR, $SCH^{Ik+:He+}$ and $SCH^{Ik-:He-}$ PBMC secretomes at DIV7, DIV14 and DIV21 (Fig. 6b). At DIV28 GcAMP6s-dependent calcium activity was recorded for 5 min in these MoNNets (Fig. 6b-c). Our results showed clear changes in activity in both groups of MoNNets treated with $SCH^{Ik+:He+}$ and $SCH^{Ik-:He-}$ secretomes compared to MoNNets treated with CTR secretome (Fig. 6d). These visual changes in activity in the raster plot were translated to a strong reduction in the average pairwise correlation, a measure of neuronal synchrony [72], in those MoNNets treated with $SCH^{Ik+:He+}$, or $SCH^{Ik-:He-}$ secretomes (Fig. 6e), which mimics what is observed in schizophrenia [97]. Interestingly, we also observed a moderate decrease in activity rate in MoNNets treated with the $SCH^{Ik+:He+}$ secretome, an effect even more robust when MoNNets were treated with the $SCH^{Ik-:He-}$ secretome (Fig. 6f). Finally, only MoNNets treated with the $SCH^{Ik-:He-}$ secretome suffered a reduction in the mean peak duration compared with the CTR condition (Fig. 6g). We concluded that, although both secretomes, the $SCH^{Ik+:He+}$ and the $SCH^{Ik-:He-}$, induced a reduction in MoNNets functional parameters (mainly synchrony) the $SCH^{Ik-:He-}$ was the one that triggered the most severe and global alterations.

IKZF1 and *IKZF2* mRNA levels in PBMCs from patients with schizophrenia modulate schizophrenia-like phenotypes with a specific impact on cognitive function

Our observations in primary neuronal cultures and in MoNNets suggested that neural networks could be influenced by an aberrant molecular profile in the PBMC secretome from patients with schizophrenia. Also, our results indicated that *IKZF1* and *IKZF2* mRNA levels modulate the severity of such impairments. Additionally, since in the double heterozygous $Ik^{\pm}$:$He^{\pm}$ mice (Figs. 2–3) both genes, *Ikzf1* and *Ikzf2*, have been genetically deleted (one allele) also in the brain, it cannot be excluded that this general deletion might have a direct effect on the synaptic plasticity in the hippocampus or other brain regions at any stage of their lifespans. Thus, we aimed to employ a different strategy to address all these points. We used a mouse line that allows a permanent tagging of neurons activated by experience or relevant stimuli: the double mutant mice expressing Egr1-CreERT2 and R26RCE (Fig. 7a) [7, 54, 80]. We permanently and intraventricularly treated these transgenic mice with pooled secretomes from CTR, $SCH^{Ik+:He+}$, and the $SCH^{Ik-:He-}$ subjects using mini-osmotic pumps for 25 days (Fig. 7b, c) at a delivery ratio of 2,5 µl/day to the lateral ventricle. We performed a broad behavioral characterization of these mice assessing the three dimensions of schizophrenia-like phenotypes [70] from day 5 to day 19 of the treatment. On day 20, mice were treated with 4-HT to induce recombination and permanent labeling of activated neural engrams due to the treatments with the secretomes. This design avoided the unspecific labeling of neural engrams due

(See figure on next page.)

Fig. 6 Impact of CTR, $SCH^{Ik+:He+}$, and $SCH^{Ik-:He-}$ supernatants in neuronal activity and synchrony. **a** Schematic overview of MoNNet approach (Left panel). Primary hippocampal cells were infected with AAV7m8.Syn.GCaMP6s.WPRE.SV40, and plated on a PDMS mold for self-organized assembly of MoNNet (a.k.a. neurospheres, Middle panel). Tuj-1 labeled MoNNets (right panel). Scale bar 250 µm. **b** The experimental design is depicted. Pooled supernatants (a.k.a. conditioned media) from each group (CTR, $SCH^{Ik+:He+}$, and $SCH^{Ik-:He-}$) of cultured PBMC were added to primary hippocampal neurons at DIV7, DIV14, and DIV21. At DIV28, their GcAMP6s-based activity was assessed. **c** Maxima projection showing GcAMP6s activity and its subsequent filtering (Gaussian > binarized > and final mask). System-wide cellular-resolution Ca^{2+} imaging was performed at 25 Hz. We analyzed the activity of each neurosphere and compared it with the rest of neurospheres. **d** Representative raster plots from DIV28 recordings in all three groups (CTR, $SCH^{Ik+:He+}$, and $SCH^{Ik-:He-}$). From the binarized signal the following parameters were computed: **e** average pairwise Pearson correlation of MoNNets (one-way ANOVA; $F_{(2, 80)} = 18,31$, $p < 0.0001$), (**f**) mean activity rate (one-way ANOVA: $F_{(2, 81)} = 10,22$, $p < 0.0001$) and (**g**) mean peak duration (one-way ANOVA: $F_{(2, 108)} = 3,893$, $p = 0.023$). In **e**–**g** one-way ANOVA was applied and the Dunnett's multiple comparisons test was used as a post hoc. *$p < 0.05$ and ***$p < 0.001$ vs CTR

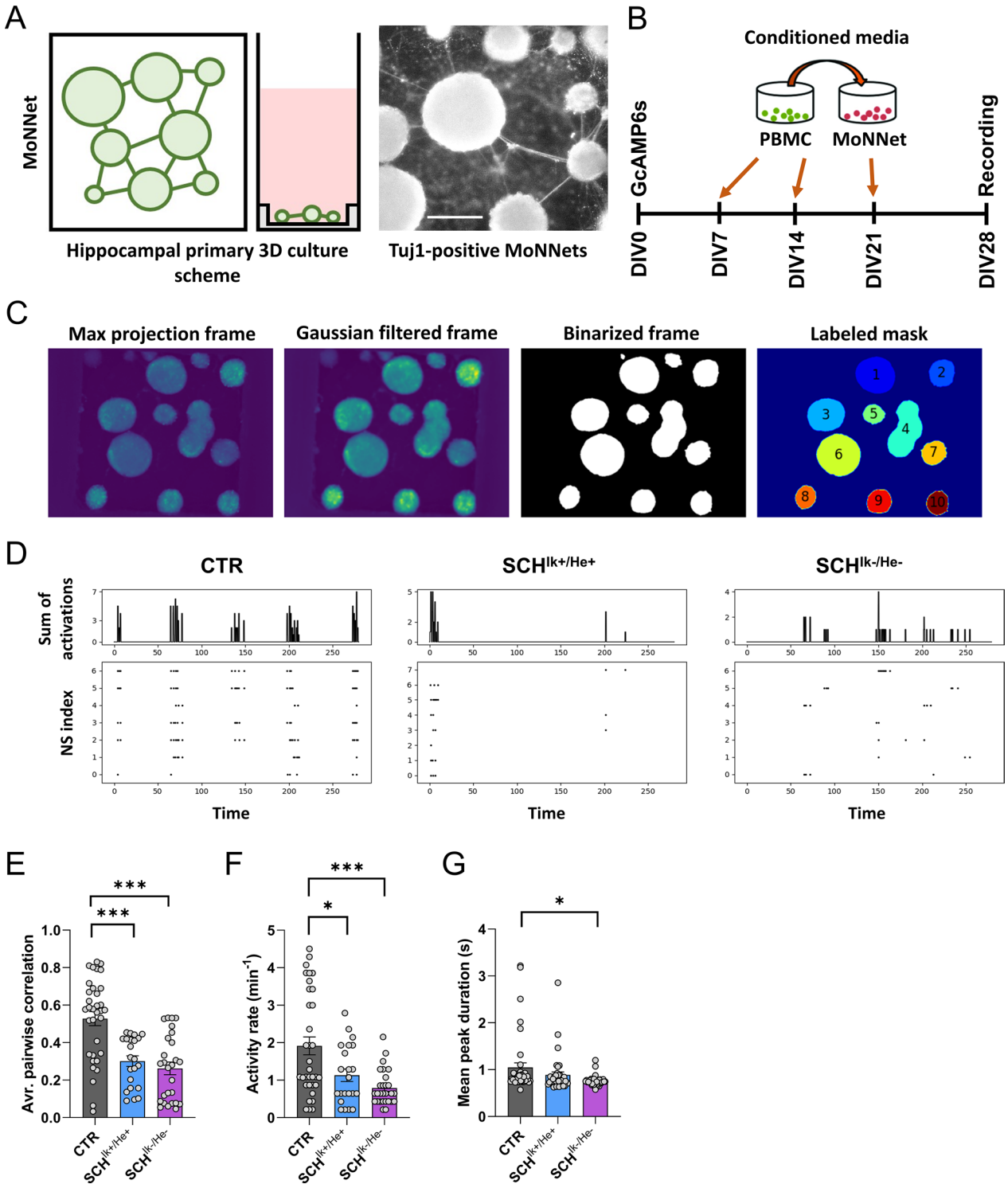

Fig. 6 (See legend on previous page.)

to the extensive behavioral characterization. Finally, brains were processed for histological studies on day 25 of treatment (Fig. 7c). Regarding the results, first, treated mice showed normal body weight (Fig. 7d) and appearance (data not shown) at the end of the study, suggesting that this treatment did not induce sickness-like states. Concerning the behavioral characterization, both $SCH^{Ik+:He+}$ and the $SCH^{Ik-:He-}$ groups showed

no changes in agitation in the open field when compared with the CTR group (Fig. 7e). In contrast, both $SCH^{Ik+:He+}$ and the $SCH^{Ik-:He-}$ groups showed a clear and equal reduction in sociability compared to the CTR group in the three-chamber social interaction test (Fig. 7f). Finally, in the novel object recognition test, the $SCH^{Ik-:He-}$ group but not the $SCH^{Ik+:He+}$ group displayed specific alterations in novel object recognition memory in comparison with the CTR group (Fig. 7g). We then mapped the activation of potential aberrant engrams due to these secretomes in fixed brains from mice of the three groups. Since cognitive alterations seemed to be highly specific to the mice treated with the $SCH^{Ik-:He-}$ secretome, we quantified the number of Egr1-dependent activated neural cells (GFP-positive) in the hippocampal CA1 (Fig. 7h) as suggested to be a core hippocampal sub-region in the physiopathology of schizophrenia [102]. We observed that, although both groups, $SCH^{Ik+:He+}$ and the $SCH^{Ik-:He-}$ displayed an apparent aberrant activation of the Egr1-dependent activated ensembles, only the mice treated with the $SCH^{Ik-:He-}$ secretome suffered a significant increase (Fig. 7h). Interestingly, increases on Egr1 levels have been previously reported in the auditory cortex [43] and in peripheral tissues of schizophrenia patients [11]. We then observed that altered structural synaptic plasticity was only detected in our mice treated with the $SCH^{Ik-:He-}$ secretome. In particular, spine density in the CA1 pyramidal neurons (Fig. 7i) but not in medium spiny neurons of the dorsal striatum (Suppl. Figure 6a) was increased in mice treated with the secretome from $SCH^{Ik-:He-}$ patients compared to the CTR group. These differences, although a trend was observed, were not significant in mice treated with the $SCH^{Ik+:He+}$ secretome. Such aberrantly increased number of Egr1-dependent activated ensembles correlated with a decrease in the number of parvalbumin-positive interneurons mostly observed in the $SCH^{Ik-:He-}$ group, but also in the $SCH^{Ik+:He+}$ group when compared with the CTR group (Fig. 7j). This reduction in parvalbumin interneurons could mediate the Egr1-dependent hyperactivation of CA1 pyramidal cells due to a lack of their inhibition [98]. Finally, because human secretomes have the potential to activate neuroinflammatory processes, we evaluated several morphometric parameters in astroglia and microglia within the same CA1 *stratum radiatum* of the mice. While human secretomes from schizophrenia patients did not alter the overall numbers of hippocampal astrocytes and microglia, they did induce morphometric changes including increased cellular solidity and increased GFAP staining (Suppl. Figure 7). Notably, the $SCH^{Ik-:He-}$ group exhibited more pronounced alterations compared to those observed in the $SCH^{Ik+:He+}$ group (Suppl. Figure 7). These findings suggest that astrocytes and microglia respond to these pathological secretomes. Overall, these results indicate that human secretomes from patients induce schizophrenia-like phenotypes in mice and that *IKZF1* and *IKZF2* levels in PBMC modulate the secretome conformation in a way that specifically impacts hippocampal activated neural ensembles likely through a reduction in parvalbumin interneurons function and ultimately impairing structural plasticity and associated cognitive skills.

(See figure on next page.)

Fig. 7 Schizophrenia-like phenotypes induced by the $SCH^{Ik+:He+}$ and $SCH^{Ik-:He-}$ supernatants when intraventricularly administered in mice. **a** Schematic representation of adult double-heterozygous-mutant Egr1-CreERT2 × R26RCE GFP mice used to label activated neural engrams upon treatment with supernatants. **b** Schematic representation of the intraventricular infusion of CTR, $SCH^{Ik+:He+}$, and $SCH^{Ik-:He-}$ supernatants. Mini-osmotic pumps infused 0,11 µl/h of supernatants at a concentration of 0,206 µg/µl of protein. **c** The experimental design is depicted. After surgical intervention, mice recovered for 4–5 days and then they were subjected to a broad behavioral characterization. At day 19, this behavioral characterization terminated and at day 20 mice were treated with 50 mg/kg of 4-hydroxytamoxifen (4-HT) to induce recombination and labeling (GFP) of activated neural ensembles. At day 25, mice were processed to evaluate neural engrams formation and labeling and to evaluate spine density in the hippocampal CA1. **d** Body weight was monitored on the day of sacrifice. **e** Basal locomotion/agitation was evaluated by using the open field in the three groups of mice (CTR, $SCH^{Ik+:He+}$, and $SCH^{Ik-:He-}$). In the same groups of mice, **f** sociability was measured using the three-chamber social interaction test/TCSIT (Group effect: $F_{(1, 102)} = 18,43$, $p < 0.0001$). **g** The same groups of mice were also subjected to the Novel Object Recognition Test/NORT (Group effect: $F_{(1, 106)} = 229,3$, $p < 0.0001$) where memory was tested 24 h after a training session. **h** Double fluorescent staining (DAPI in blue, GFP in green) in hippocampal CA1 from mice treated with one of each supernatant (CTR, $SCH^{Ik+:He+}$, and $SCH^{Ik-:He-}$). Graph (right-down) shows quantification of Egr1-dependent activated CA1 pyramidal cells (estimated number of GFP-positive cells/area of 500 μm^2, Group effect: $F_{(2, 22)} = 3,926$, $p = 0.034$). Scale bar, 300 µm. **i** Representative images and quantification (right-down panel) of spine density in secondary apical dendrites of the CA1 pyramidal neurons labeled with Golgi staining (n = 72–121 dendrites/group from 7 mice/group). Images were obtained in a bright-field microscope in the three groups of mice treated with CTR, $SCH^{Ik+:He+}$, and $SCH^{Ik-:He-}$ supernatants (Scale bar, 5 µm). **j** Double fluorescent staining (left panels, DAPI in blue, parvalbumin in red) in hippocampal CA1 from the same mice as in **h**. Graph (right) shows quantification of parvalbumin-positive interneurons in the CA1 (estimated number of parvalbumin-positive cells/area of 500 μm^2, Group effect: $F_{(2, 27)} = 33,86$, $p < 0.001$). Scale bar, 300 µm. Data are means ± SEM. In **d**, **h** and **l** one-way ANOVA was applied, and Tukey's multiple comparisons test was used as a post hoc. In **e**, **f**, and **g**, two-way ANOVA was applied, and Bonferroni's multiple comparisons test was used as a post hoc. *$p < 0.05$, vs CTR; ***$p < 0.001$, vs Empty or vs Old Object. CTR (n = 18); $SCH^{Ik+:He+}$ (n = 20); $SCH^{Ik-:He-}$ (n = 18). In **j** n = 10 in all groups

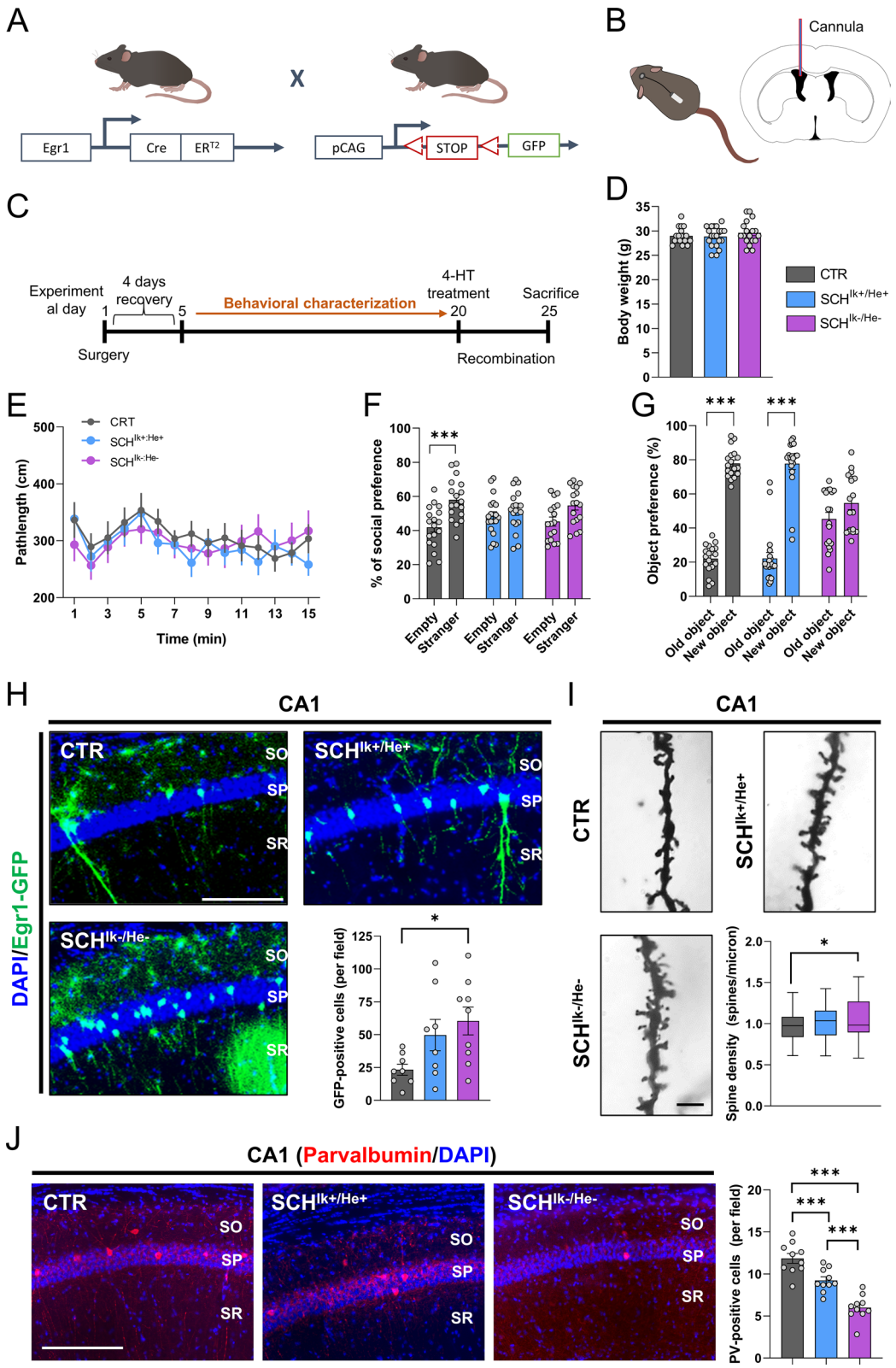

Fig. 7 (See legend on previous page.)

Discussion

In the present work, we show for the first time that both, *IKZF1* and *IKZF2*, are downregulated specifically in immune circulating cells, but not in the brains of patients with schizophrenia. We also observed in mice that a double *Ikzf1* and *Ikzf2* heterozygosis induced schizophrenia-like symptoms in the three dimensions (positive–negative-cognitive) of symptomatology. Exploring the secretome of these circulating immune cells, we observed that high-order cognitive functions are the most susceptible to be affected by the double *IKZF1* and *IKZF2* reduction. Specific and acutely hyperactivated hippocampal engrams, reduced number of parvalbumin interneurons and altered neuronal synchrony were associated with these phenotypes placing molecules such as IL-4 and CXCL10 as potential core signals mediating them.

First, we show that *IKZF1* and *IKZF2* mRNA levels are specifically downregulated in CD4 + cells but not in CD8 + cells. Such specific double down-regulation could induce changes on numbers of CD4 + cells and, in turn, to provoke differences on CD4 + /CD8 + ratios [16, 90]. Also, a double down-regulation of *IKZF1* and *IKZF2* mRNA levels in CD4 cells could provoke an imbalance between T helper cell type 1 (Th1) and type 2 (Th2) which has been associated with schizophrenia [107]. Interestingly, this imbalance has also been associated to a decrease on IL-4 expression in Th2 cells in schizophrenia patients [68] which is in line with our results on IL-4 levels. This imbalance reinforces the idea about the production of aberrant secretomes by these immune cells (which might be explained, at least in part, by this *IKZF1-IKZF2* double downregulation) and that it would correlate with more severe symptoms and poor therapy outcomes [85] as we observed in our mouse models.

Regarding the impaired secretomes, previous reports have already addressed the molecular profile of PBMCs in patients with schizophrenia [26, 103]. Despite these previous studies and as far as we know, we show for the first time a double down-regulation of *IKZF1* and *IKZF2* mRNA levels. Interestingly, these and other studies have found that WNT signaling is a core pathway affected in these cells and that there is a correlation between WNT signaling and cognitive impairment in schizophrenia [103]. In this line, the WNT family strongly regulates the *IKZF* genes in immune cells [104, 105], being a potential source of this double affectation of *IKZF1* and *IKZF2*. Regarding the cause of this double down-regulation, a plausible possibility is that alterations in *IKZF1* and *IKZF2* mRNA levels are indirectly provoked by other processes, such as immune and/or environmental challenges, as it has been proposed for the disorder [20]. Also, it is noteworthy that secretomes specifically from CD4 +, the cell type suffering of the double *IKZF1-IKZF2* downregulation, could be the major source of phenotypes observed in our in vitro and in vivo models. This could be a very promising future line of research.

To demonstrate the relevance of this double downregulation as a potential underlying molecular mechanism explaining the pathophysiology of schizophrenia, we have used both, a genetic and a translational model. In the genetic model, we have observed a highly schizophrenia-like phenotype (with phenotypes in all three dimensions, positive–negative-cognitive) in mice in terms of behavior and neuronal changes. However, although our data support the idea that an *Ikzf1-Ikzf2* double reduction is necessary to display a full three-dimensional schizophrenia-like phenotype, it is worth mentioning that heterozygous $Ik^{\pm}$:$He^{+/+}$ and $Ik^{+/+}$:$He^{\pm}$ mice also display some specific schizophrenia-like phenotypes. This indicates that the observed phenotypes induced by the double reduction are partly synergistic but also partly additive. Besides, in this mouse model, we have explored potential sex differences which were worse in males than in females. Regarding these sex differences, it has been previously reported that in human beings, males and females show differences in terms of pathology and prevalence being worse in males [50]. Concerning cognitive dysfunction, male patients perform worse on measures of executive function, verbal memory and information processing speed than female patients [63] which is in line with our results in our mouse models. Thus, since there are also sex-dependent immune alterations in schizophrenia patients [39, 46, 108], probably the double *IKZF1-IKZF2* double downregulation affects more males than females in terms of some behavioral and neuropathological phenotypes. Regarding the translational model in which we used PBMC secretomes from patients, we concluded that an aberrant immune secretome with a double reduction of *IKZF1* and *IKZF2* from schizophrenia patients is enough to induce negative-like and cognitive-like symptoms. These results are in line with the idea that immune alterations are highly associated with such types of symptoms [32, 58, 76]. Noteworthy, the fact we did not observe differences in agitation in such translational mouse models could be because PBMC' secretomes came from patients under treatment with antipsychotics. Although this statement is just speculative, it is in line with the large evidence stating that antipsychotics target principally positive symptoms whereas negative and cognitive symptoms remain largely unaffected [58]. Shall our hypothesis be true it would reinforce the fact of using agitation in mice as a positive-like phenotype/parameter.

Since our human PBMC secretomes induced so many schizophrenia-like phenotypes in terms of structural synaptic plasticity [66], neuronal synchrony [72], and

schizophrenia-like behaviors [70], we then explored their molecular profile. We first found that levels of RANTES (CCL5), an upregulated cytokine in schizophrenia [19, 22], depended on *IKZF1* and *IKZF2* levels. However, the role of RANTES in schizophrenia is largely unknown. Another promising core molecule is IL-4. IL-4 rises as an interesting molecule coordinating the specific neuronal and cognitive symptoms observed in the induced SCH $^{Ik-/He-}$ in vitro and in vivo models. IL-4 is an attractive candidate since its levels are regulated by both, *IKZF1* and *IKZF2* in circulating immune cells [34, 53, 71, 106]. Second, IL-4 regulates hippocampal-dependent memory [8, 24], and deficiency of its receptor, IL-4R, increased network activity [36] similar to what we observed in the hippocampus of our in vivo induced SCH $^{Ik-/He-}$ mouse model. In the context of schizophrenia, IL-4 has been shown to be significantly decreased in chronic schizophrenia-spectrum [35]. Furthermore, some single nucleotide polymorphisms (SNPs) in IL-4 have been related to the disorder [84]. Additional studies have also shown that IL-4 levels are not related to positive psychotic symptoms [21] but, instead, they correlate with negative symptoms [88]. A third plausible candidate molecule underlying the defects observed in our SCH $^{Ik-/He-}$ mice is CXCL10 (IP10). Supporting this idea previous studies have observed enhanced neural activity accompanied by increased firing rate and excitability and alterations in synaptic network activity after chronic treatment with CXCL10 [13, 67]. These changes were sustained by reduced levels of GABA receptors, augmented levels of glutamate receptors and increased sensitivity of NMDA receptors [13, 67]. All these findings go in line with; the enhanced hippocampal Egr1-dependent activated ensembles in our SCH $^{Ik-/He-}$ mice, the basal hyperexcitability normally seen in schizophrenia patients and the reduced synchronized neural activity present in schizophrenia patients and in our SCH $^{Ik-/He-}$ in vitro MoNNet model. In this line, previous works [33, 89] have already proposed the hyperexcitability of the hippocampus as a core feature contributing to the three categories of symptoms seen in schizophrenia (Suppl Fig. 7a-c). We propose that our $Ik^{\pm}$:$He^{\pm}$ and SCH $^{Ik-/He-}$ models provide key underlying molecular clues, including IL-4 and CXCL10, supporting this model. As it has been reported in patients with schizophrenia [48], we also observed a reduction of parvalbumin-positive interneurons (PV+) in the hippocampal CA1 in our SCH $^{Ik-/He-}$ model. This reduction could be provoked by aberrant levels of IL-4 and CXCL10 from circulating PBMCs with decreased *IKZF1* and *IKZF2* levels. This altered secretome would induce a reduction in PV+cells number and/or function since it has been shown that IL-4 reduces the risk of hyperexcitation [36] and CXCL10 over-expression reduces the levels of GAD65/67 [13] often accompanied of a ferroptosis processes [51]. The reduced function of PV+interneurons would provoke an hyperactivation of pyramidal neurons in the CA1 according to this circuit [98] and ultimately inducing the deficits in structural plasticity and impairments in cognitive function. However, although we provide evidences for this model, we cannot rule out other components allocated in these aberrant secretomes such as small molecules (RNAs) or extracellular vesicles [3, 42]. Future studies could address such possibilities. Finally, although the main effect mediated by the immune secretomes from schizophrenia patients was observed in the parvalbumin interneurons, we also observed some morphological changes in astroglia and microglia suggesting that such changes could also play a role in the synaptic plasticity alterations and associated cognitive and social deficits observed in our intraventricularly injected mice. Indeed, aberrant activation of microglia [59, 100] or astroglia [93] could alter the function of parvalbumin interneurons in the hippocampus.

Our study has important limitations, particularly regarding human samples. First, we focused on mRNA levels in human PBMCs to evaluate *IKZF1* and *IKZF2* expression; however, the protein-level results for *IKZF2* did not fully corroborate the mRNA findings. It is well-established that discrepancies often arise when comparing mRNA and protein levels [49, 73], potentially due to greater variability in protein expression [56]. Therefore, the role of *IKZF2* in our findings should be interpreted with caution. Still with human samples, there is a discrepancy in the number of recruited controls (CTR) and patients with schizophrenia (SCH) in the same experiments using PBMCs, which could introduce bias. Also, patients for the secretome experiments were matched in terms of *IKZF1-IKZF2* mRNA levels but medication was not considered. Finally, we cannot rule out possible effects on neural *IKZF1* and *IKZF2* levels during earlier stages of the disorder since postmortem samples were collected from very old individuals, whereas PBMCs were collected from younger patients. In those same postmortem samples, there were other potential limitations such as differences in the postmortem time intervals and sex discrepancies in terms of proportions in each group. Therefore, although our results are supported by our studies using in vivo and in vitro models, the human data should be interpreted with caution.

Finally, our work fits with the idea that neural identities and probably function are both strongly modulated by peripheral signals and influences [55, 92] as we summarized (Suppl Fig. 8). One of them could be a double down-regulation of *IKZF1* and *IKZF2* mRNA levels in immune cells. In this sense, our results also have potential clinical implications. First, they could contribute to

a better definition and stratification of patients based on their blood mRNA levels of *IKZF1* and *IKZF2*, which could be related to the severity of some symptoms. Additionally, it is tempting to speculate that different types of therapeutic strategies (drugs, RNA probes, Adeno-Associated Virus/AAVs) aimed at increasing mRNA levels of these transcription factors in circulating PBMCs could have positive therapeutic effects in patients with schizophrenia. Therefore, we strongly believe that future research should progress in the study of peripheral signals capable to play a role in the development of symptoms in schizophrenia and, probably, in other psychiatric affectations.

Supplementary Information

The online version contains supplementary material available at https://doi.org/10.1186/s12974-024-03320-3.

Supplementary material 1.

Acknowledgements
We thank María Calvo from the Advanced Microscopy Service (Centres Científics i Tecnològics Universitat de Barcelona) for her help in the acquisition, analysis, and interpretation of the confocal images.

Author contribution
Ivan Ballasch and Laura López-Molina: writing—review & editing, writing—original draft, visualization, validation, methodology, investigation, formal analysis, data curation, conceptualization. Sara Borràs-Pernas, Irene Rodríguez-Navarro, Anna Sancho-Balsells and Marcos Galán-Ganga: methodology, investigation, formal analysis. Angeles Rabadan, Wanqi Chen, Carla Hernández, Miqueu Alfonso, Natalia Egri, Francesca Flotta, Wang Maoyu and Carlota Pastó-Pellicer: investigation, formal analysis. Carlota Dobaño and Ruth Aguilar: resources, formal analysis. Enrique Santamaría and Joaquín Irigoyen: investigation and data curation. Daniel del Toro: resources, writing—review & editing. Jordi Alberch and Manel Juan: supervision, resources. Josep-Maria Canals and Belén Arranz: writing—review & editing, supervision, resources, conceptualization. Albert Giralt: writing—review & editing, visualization, validation, supervision, resources, project administration, funding acquisition, conceptualization.

Funding
This work was supported by grants from Ministerio de Ciencia e Innovación/AEI/https://doi.org/10.13039/501100011033/ and "FEDER" to A.G.: PID2021-122258OB-I00 and to J.A.: PID2020-119386RB-100 and from Instituto de Salud Carlos III (ISCIII): PI17/00246 to B.A. Our technician Ana López, was supported by a María de Maeztu Unit of Excellence (Institute of Neurosciences, University of Barcelona, CEX2021-001159-M, Ministry of Science and Innovation). The project that gave rise to these results received the support of a fellowship from "la Caixa" Foundation (ID 100010434). The fellowship code is LCF/BQ/DR21/11880016 to M.G.-G.

Data availability
No datasets were generated or analysed during the current study.

Declarations

Ethics approval and consent to participate
All the procedures for the obtention of post-mortem samples followed the ethical guidelines of the Declaration of Helsinki and local ethical committees (Universitat de Barcelona: IRB00003099; Fundació CEIC Sant Joan de Déu: BTN-PSSJD). The blood samples of this study (N∘PI17/00246, PI Belen Arranz) was recruited in the Outpatient clinic located in Cornellà, Barcelona, Spain (Parc Sanitari Sant Joan de Deu). All animal procedures were approved by local committees [Universitat de Barcelona, CEEA (136/19); Generalitat de Catalunya (DAAM 10786) following the European Communities Council Directive (86/609/EU).

Competing interests
The authors declare no competing interests.

Received: 21 June 2024 Accepted: 6 December 2024
Published online: 18 December 2024

References

1. Aguilar R, Campo JJ, Chicuecue S, Cisteró P, Català A, Luis L, Ubillos I, Galatas B, Aide P, Guinovart C, Moncunill G, Dobaño C. Changing plasma cytokine, chemokine and growth factor profiles upon differing malaria transmission intensities. Malar J. 2019;18:406. https://doi.org/10.1186/s12936-019-3038-x.
2. Ahmad SF, Nadeem A, Ansari MA, Bakheet SA, AL-Ayadhi LY, Attia SM. Downregulation in Helios transcription factor signaling is associated with immune dysfunction in blood leukocytes of autistic children. Prog Neuro-Psychopharmacol Biol Psychiatry. 2018;85:98–104. https://doi.org/10.1016/j.pnpbp.2018.04.011.
3. Alberro A, Iparraguirre L, Fernandes A, Otaegui D. Extracellular vesicles in blood: sources, effects, and applications. Int J Mol Sci. 2021;22:8163. https://doi.org/10.3390/ijms22158163.
4. Alhosaini K, Ansari MA, Nadeem A, Attia SM, Bakheet SA, Al-Ayadhi LY, Mahmood HM, Al-Mazroua HA, Ahmad SF. Dysregulation of Ki-67 expression in T cells of children with autism spectrum disorder. Children. 2021;8:116. https://doi.org/10.3390/children8020116.
5. Alsiö JM, Tarchini B, Cayouette M, Livesey FJ. Ikaros promotes early-born neuronal fates in the cerebral cortex. Proc Natl Acad Sci. 2013. https://doi.org/10.1073/pnas.1215707110.
6. Ballasch I, García-García E, Vila C, Pérez-González A, Sancho-Balsells A, Fernández J, Soto D, Puigdellívol M, Gasull X, Alberch J, Rodríguez MJ, Canals JM, Giralt A. Ikzf1 as a novel regulator of microglial homeostasis in inflammation and neurodegeneration. Brain Behav Immun. 2023;109:144–61. https://doi.org/10.1016/j.bbi.2023.01.016.
7. Brito V, Montalban E, Sancho-Balsells A, Pupak A, Flotta F, Masana M, Ginés S, Alberch J, Martin C, Girault J-A, Giralt A. Hippocampal Egr1-dependent neuronal ensembles negatively regulate motor learning. J Neurosci. 2022;42:5346–60. https://doi.org/10.1523/JNEUROSCI.2258-21.2022.
8. Brombacher TM, Berkiks I, Pillay S, Scibiorek M, Moses BO, Brombacher F. IL-4R alpha deficiency influences hippocampal-BDNF signaling pathway to impair reference memory. Sci Rep. 2020;10:16506. https://doi.org/10.1038/s41598-020-73574-3.
9. Busse S, Busse M, Schiltz K, Bielau H, Gos T, Brisch R, Mawrin C, Schmitt A, Jordan W, Müller UJ, Bernstein H-G, Bogerts B, Steiner J. Different distribution patterns of lymphocytes and microglia in the hippocampus of patients with residual versus paranoid schizophrenia: further evidence for disease course-related immune alterations? Brain Behav Immun. 2012;26:1273–9. https://doi.org/10.1016/j.bbi.2012.08.005.
10. Cai Q, Dierich A, Oulad-Abdelghani M, Chan S, Kastner P. Helios deficiency has minimal impact on T cell development and function. J Immunol. 2009;183:2303–11. https://doi.org/10.4049/jimmunol.0901407.
11. Cattane N, Minelli A, Milanesi E, Maj C, Bignotti S, Bortolomasi M, Chiavetto LB, Gennarelli M. Altered gene expression in schizophrenia: findings from transcriptional signatures in fibroblasts and blood. PLoS ONE. 2015;10: e0116686. https://doi.org/10.1371/journal.pone.0116686.
12. Chaudhry IB, Husain MO, Khoso AB, Husain MI, Buch MH, Kiran T, Fu B, Bassett P, Qurashi I, ur Rahman R, Baig S, Kazmi A, Corsi-Zuelli F, Haddad PM, Deakin B, Husain N. A randomised clinical trial of methotrexate points to possible efficacy and adaptive immune dysfunction in psychosis. Transl Psychiatry. 2020;10:415. https://doi.org/10.1038/s41398-020-01095-8.
13. Cho J, Nelson TE, Bajova H, Gruol DL. Chronic CXCL10 alters neuronal properties in rat hippocampal culture. J Neuroimmunol. 2009;207:92–100. https://doi.org/10.1016/j.jneuroim.2008.12.007.

14. Consortium A.W.G. of T.P.G. Meta-analysis of GWAS of over 16,000 individuals with autism spectrum disorder highlights a novel locus at 10q24.32 and a significant overlap with schizophrenia. Mol Autism. 2017;8:21. https://doi.org/10.1186/s13229-017-0137-9.
15. Corsi-Zuelli F, Deakin B, de Lima MHF, Qureshi O, Barnes NM, Upthegrove R, Louzada-Junior P, Del-Ben CM. T regulatory cells as a potential therapeutic target in psychosis? Current challenges and future perspectives. Brain Behav Immun Heal. 2021;17:100330. https://doi.org/10.1016/j.bbih.2021.100330.
16. Craddock RM, Lockstone HE, Rider DA, Wayland MT, Harris LJW, McKenna PJ, Bahn S. Altered T-cell function in schizophrenia: a cellular model to investigate molecular disease mechanisms. PLoS ONE. 2007;2:e692. https://doi.org/10.1371/journal.pone.0000692.
17. Davis J, Eyre H, Jacka FN, Dodd S, Dean O, McEwen S, Debnath M, McGrath J, Maes M, Amminger P, McGorry PD, Pantelis C, Berk M. A review of vulnerability and risks for schizophrenia: beyond the two hit hypothesis. Neurosci Biobehav Rev. 2016;65:185–94. https://doi.org/10.1016/j.neubiorev.2016.03.017.
18. de Pins B, Cifuentes-Díaz C, Thamila Farah A, López-Molina L, Montalban E, Sancho-Balsells A, López A, Ginés S, Delgado-García JM, Alberch J, Gruart A, Girault J-A, Giralt A. Conditional BDNF delivery from astrocytes rescues memory deficits, spine density and synaptic properties in the 5xFAD mouse model of Alzheimer disease. J Neurosci. 2019. https://doi.org/10.1523/JNEUROSCI.2121-18.2019.
19. Domenici E, Willé DR, Tozzi F, Prokopenko I, Miller S, McKeown A, Brittain C, Rujescu D, Giegling I, Turck CW, Holsboer F, Bullmore ET, Middleton L, Merlo-Pich E, Alexander RC, Muglia P. Plasma protein biomarkers for depression and schizophrenia by multi analyte profiling of case-control collections. PLoS ONE. 2010;5: e9166. https://doi.org/10.1371/journal.pone.0009166.
20. Ermakov EA, Melamud MM, Buneva VN, Ivanova SA. Immune system abnormalities in schizophrenia: an integrative view and translational perspectives. Front Psychiatry. 2022. https://doi.org/10.3389/fpsyt.2022.880568.
21. Fila-Danilow A, Kucia K, Kowalczyk M, Owczarek A, Paul-Samojedny M, Borkowska P, Suchanek R, Kowalski J. Association study of interleukin-4 polymorphisms with paranoid schizophrenia in the Polish population: a critical approach. Mol Biol Rep. 2012;39:7941–7. https://doi.org/10.1007/s11033-012-1639-3.
22. Frydecka D, Krzystek-Korpacka M, Lubeiro A, Stramecki F, Stańczykiewicz B, Beszłej JA, Piotrowski P, Kotowicz K, Szewczuk-Bogusławska M, Pawlak-Adamska E, Misiak B. Profiling inflammatory signatures of schizophrenia: a cross-sectional and meta-analysis study. Brain Behav Immun. 2018;71:28–36. https://doi.org/10.1016/j.bbi.2018.05.002.
23. Furney SJ, Simmons A, Breen G, Pedroso I, Lunnon K, Proitsi P, Hodges A, Powell J, Wahlund L-O, Kloszewska I, Mecocci P, Soininen H, Tsolaki M, Vellas B, Spenger C, Lathrop M, Shen L, Kim S, Saykin AJ, Weiner MW, Lovestone S. Genome-wide association with MRI atrophy measures as a quantitative trait locus for Alzheimer's disease. Mol Psychiatry. 2011;16:1130–8. https://doi.org/10.1038/mp.2010.123.
24. Gadani SP, Cronk JC, Norris GT, Kipnis J. IL-4 in the brain: a cytokine to remember. J Immunol. 2012;189:4213–9. https://doi.org/10.4049/jimmunol.1202246.
25. Gao Y, Li J, Cai G, Wang Y, Yang W, Li Y, Zhao X, Li R, Gao Y, Tuo W, Baldwin RL, Li C, Fang L, Liu GE. Single-cell transcriptomic and chromatin accessibility analyses of dairy cattle peripheral blood mononuclear cells and their responses to lipopolysaccharide. BMC Genom. 2022;23:338. https://doi.org/10.1186/s12864-022-08562-0.
26. Gardiner EJ, Cairns MJ, Liu B, Beveridge NJ, Carr V, Kelly B, Scott RJ, Tooney PA. Gene expression analysis reveals schizophrenia-associated dysregulation of immune pathways in peripheral blood mononuclear cells. J Psychiatr Res. 2013;47:425–37. https://doi.org/10.1016/j.jpsychires.2012.11.007.
27. Georgopoulos K, Winandy S, Avitahl N. The role of the ikaros gene in lymphocyte development and homeostasis. Annu Rev Immunol. 1997;15:155–76. https://doi.org/10.1146/annurev.immunol.15.1.155.
28. Giralt A, Brito V, Chevy Q, Simonnet C, Otsu Y, Cifuentes-Díaz C, de Pins B, Coura R, Alberch J, Ginés S, Poncer J-C, Girault J-A. Pyk2 modulates hippocampal excitatory synapses and contributes to cognitive deficits in a Huntington's disease model. Nat Commun. 2017;8:15592. https://doi.org/10.1038/ncomms15592.
29. Giralt A, Brito V, Pardo M, Rubio SE, Marion-Poll L, Martín-Ibáñez R, Zamora-Moratalla A, Bosch C, Ballesteros JJ, Blasco E, García-Torralba A, Pascual M, Pumarola M, Alberch J, Ginés S, Martín ED, Segovia J, Soriano E, Canals JM. Helios modulates the maturation of a CA1 neuronal subpopulation required for spatial memory formation. Exp Neurol. 2020;323:113095. https://doi.org/10.1016/j.expneurol.2019.113095.
30. Glausier JR, Lewis DA. Dendritic spine pathology in schizophrenia. Neuroscience. 2013;251:90–107. https://doi.org/10.1016/j.neuroscience.2012.04.044.
31. Goldsmith DR, Haroon E, Miller AH, Strauss GP, Buckley PF, Miller BJ. TNF-α and IL-6 are associated with the deficit syndrome and negative symptoms in patients with chronic schizophrenia. Schizophr Res. 2018;199:281–4. https://doi.org/10.1016/j.schres.2018.02.048.
32. Goldsmith DR, Rapaport MH. Inflammation and negative symptoms of schizophrenia: implications for reward processing and motivational deficits. Front Psychiatry. 2020. https://doi.org/10.3389/fpsyt.2020.00046.
33. Grace AA, Gomes FV. The circuitry of dopamine system regulation and its disruption in schizophrenia: insights into treatment and prevention. Schizophr Bull. 2019;45:148–57. https://doi.org/10.1093/schbul/sbx199.
34. Gregory GD. Mast cell IL-4 expression is regulated by Ikaros and influences encephalitogenic Th1 responses in EAE. J Clin Invest. 2006;116:1327–36. https://doi.org/10.1172/JCI27227.
35. Halstead S, Siskind D, Amft M, Wagner E, Yakimov V, Shih-Jung Liu Z, Walder K, Warren N. Alteration patterns of peripheral concentrations of cytokines and associated inflammatory proteins in acute and chronic stages of schizophrenia: a systematic review and network meta-analysis. Lancet Psychiatry. 2023;10:260–71. https://doi.org/10.1016/S2215-0366(23)00025-1.
36. Hanuscheck N, Thalman C, Domingues M, Schmaul S, Muthuraman M, Hetsch F, Ecker M, Endle H, Oshaghi M, Martino G, Kuhlmann T, Bozek K, van Beers T, Bittner S, von Engelhardt J, Vogt J, Vogelaar CF, Zipp F. Interleukin-4 receptor signaling modulates neuronal network activity. J Exp Med. 2022. https://doi.org/10.1084/jem.20211887.
37. Harding BN, Aguilar R, Espinosa A, Castaño-Vinyals G, Papantoniou K, Navarrete JM, Such Faro P, Torrejón A, Dobaño C, Moncunill G, Kogevinas M. Disruption of cellular immune response among male rotating night shift workers in Spain– The HORMONIT study. Front Immunol. 2022. https://doi.org/10.3389/fimmu.2022.776917.
38. Harrison PJ. Neuropathology of schizophrenia. Psychiatry. 2008;7:421–4. https://doi.org/10.1016/j.mppsy.2008.07.013.
39. He J, Wei Y, Li J, Tang Y, Liu J, He Z, Zhou R, He X, Ren H, Liao Y, Gu L, Yuan N, Chen X, Tang J. Sex differences in the association of treatment-resistant schizophrenia and serum interleukin-6 levels. BMC Psychiatry. 2023;23:470. https://doi.org/10.1186/s12888-023-04952-0.
40. Homann J, Osburg T, Ohlei O, Dobricic V, Deecke L, Bos I, Vandenberghe R, Gabel S, Scheltens P, Teunissen CE, Engelborghs S, Frisoni G, Blin O, Richardson JC, Bordet R, Lleó A, Alcolea D, Popp J, Clark C, Peyratout G, Martinez-Lage P, Tainta M, Dobson RJB, Legido-Quigley C, Sleegers K, Van Broeckhoven C, Wittig M, Franke A, Lill CM, Blennow K, Zetterberg H, Lovestone S, Streffer J, ten Kate M, Vos SJB, Barkhof F, Visser PJ, Bertram L. Genome-wide association study of Alzheimer's disease brain imaging biomarkers and neuropsychological phenotypes in the European medical information framework for Alzheimer's disease multimodal biomarker discovery dataset. Front Aging Neurosci. 2022. https://doi.org/10.3389/fnagi.2022.840651.
41. Houthuys E, Movahedi K, De Baetselier P, Van Ginderachter JA, Brouckaert P. A method for the isolation and purification of mouse peripheral blood monocytes. J Immunol Methods. 2010;359:1–10. https://doi.org/10.1016/j.jim.2010.04.004.
42. Hunter MP, Ismail N, Zhang X, Aguda BD, Lee EJ, Yu L, Xiao T, Schafer J, Lee M-LT, Schmittgen TD, Nana-Sinkam SP, Jarjoura D, Marsh CB. Detection of microRNA expression in human peripheral blood microvesicles. PLoS ONE. 2008;3: e3694. https://doi.org/10.1371/journal.pone.0003694.
43. Iwakura Y, Kawahara-Miki R, Kida S, Sotoyama H, Gabdulkhaev R, Takahashi H, Kunii Y, Hino M, Nagaoka A, Izumi R, Shishido R, Someya T, Yabe H, Kakita A, Nawa H. Elevation of EGR1/zif268, a neural activity marker, in the auditory cortex of patients with schizophrenia and its animal

model. Neurochem Res. 2022;47:2715–27. https://doi.org/10.1007/s11064-022-03599-9.
44. John LB, Ward AC. The ikaros gene family: transcriptional regulators of hematopoiesis and immunity. Mol Immunol. 2011;48:1272–8. https://doi.org/10.1016/j.molimm.2011.03.006.
45. Johnsen E, Fathian F, Kroken RA, Steen VM, Jørgensen HA, Gjestad R, Løberg E-M. The serum level of C-reactive protein (CRP) is associated with cognitive performance in acute phase psychosis. BMC Psychiatry. 2016;16:60. https://doi.org/10.1186/s12888-016-0769-x.
46. Kamitaki N, Sekar A, Handsaker RE, de Rivera H, Tooley K, Morris DL, Taylor KE, Whelan CW, Tombleson P, Loohuis LMO, Boehnke M, Kimberly RP, Kaufman KM, Harley JB, Langefeld CD, Seidman CE, Pato MT, Pato CN, Ophoff RA, Graham RR, Criswell LA, Vyse TJ, McCarroll SA. Complement genes contribute sex-biased vulnerability in diverse disorders. Nature. 2020;582:577–81. https://doi.org/10.1038/s41586-020-2277-x.
47. Kleiveland CR. Peripheral blood mononuclear cells. In: The impact of food bioactives on health. Cham: Springer International Publishing; 2015. p. 161–7. https://doi.org/10.1007/978-3-319-16104-4_15.
48. Konradi C, Yang CK, Zimmerman EI, Lohmann KM, Gresch P, Pantazopoulos H, Berretta S, Heckers S. Hippocampal interneurons are abnormal in schizophrenia. Schizophr Res. 2011;131:165–73. https://doi.org/10.1016/j.schres.2011.06.007.
49. Li J, Han S, Li H, Udeshi ND, Svinkina T, Mani DR, Xu C, Guajardo R, Xie Q, Li T, Luginbuhl DJ, Wu B, McLaughlin CN, Xie A, Kaewsapsak P, Quake SR, Carr SA, Ting AY, Luo L. Cell-surface proteomic profiling in the fly brain uncovers wiring regulators. Cell. 2020;180:373-386.e15. https://doi.org/10.1016/j.cell.2019.12.029.
50. Li X, Zhou W, Yi Z. A glimpse of gender differences in schizophrenia. Gen psychiatry. 2022;35: e100823. https://doi.org/10.1136/gpsych-2022-100823.
51. Liang P, Zhang X, Zhang Y, Wu Y, Song Y, Wang X, Chen T, Liu W, Peng B, Yin J, He F, Fan Y, Han S, He X. Neurotoxic A1 astrocytes promote neuronal ferroptosis via CXCL10/CXCR3 axis in epilepsy. Free Radic Biol Med. 2023;195:329–42. https://doi.org/10.1016/j.freeradbiomed.2023.01.002.
52. Liemburg EJ, Nolte IM, Klein HC, Knegtering H. Relation of inflammatory markers with symptoms of psychotic disorders: a large cohort study. Prog Neuro-Psychopharmacol Biol Psychiatry. 2018;86:89–94. https://doi.org/10.1016/j.pnpbp.2018.04.006.
53. Long Y, Xia C, Xu L, Liu C, Fan C, Bao H, Zhao X, Liu C. The imbalance of circulating follicular helper T cells and follicular regulatory T cells is associated with disease activity in patients with ulcerative colitis. Front Immunol. 2020. https://doi.org/10.3389/fimmu.2020.00104.
54. Longueville S, Nakamura Y, Brami-Cherrier K, Coura R, Hervé D, Girault J. Long-lasting tagging of neurons activated by seizures or cocaine administration in Egr1-CreER T2 transgenic mice. Eur J Neurosci. 2021;53:1450–72. https://doi.org/10.1111/ejn.15060.
55. López M, Tovar S, Vázquez MJ, Williams LM, Diéguez C. Peripheral tissue–brain interactions in the regulation of food intake. Proc Nutr Soc. 2007;66:131–55. https://doi.org/10.1017/S0029665107005368.
56. Luo J, Li L, Niu M, Kong D, Jiang Y, Poudel S, Shieh AW, Cheng L, Giase G, Grennan K, White KP, Chen C, Wang SH, Pinto D, Wang Y, Liu C, Peng J, Wang X. Genetic regulation of human brain proteome reveals proteins implicated in psychiatric disorders. Mol Psychiatry. 2024;29:3330–43. https://doi.org/10.1038/s41380-024-02576-8.
57. MacDowell KS, Munarriz-Cuezva E, Caso JR, Madrigal JLM, Zabala A, Meana JJ, García-Bueno B, Leza JC. Paliperidone reverts Toll-like receptor 3 signaling pathway activation and cognitive deficits in a maternal immune activation mouse model of schizophrenia. Neuropharmacology. 2017;116:196–207. https://doi.org/10.1016/j.neuropharm.2016.12.025.
58. Malashenkova IK, Ushakov VL, Zakharova NV, Krynskiy SA, Ogurtsov DP, Hailov NA, Chekulaeva EI, Ratushnyy AY, Kartashov SI, Kostyuk GP, Didkovsky NA. Neuro-immune aspects of schizophrenia with severe negative symptoms: new diagnostic markers of disease phenotype. Sovrem Tehnol Med. 2021. https://doi.org/10.17691/stm2021.13.6.03.
59. Mao M, Zhou Z, Sun M, Wang C, Sun J. The dysfunction of parvalbumin interneurons mediated by microglia contributes to cognitive impairment induced by lipopolysaccharide challenge. Neurosci Lett. 2021;762:136133. https://doi.org/10.1016/j.neulet.2021.136133.
60. Martín-Ibáñez R, Pardo M, Giralt A, Miguez A, Guardia I, Marion-Poll L, Herranz C, Esgleas M, Barriga GG-D, Edel MJ, Vicario-Abejón C, Alberch J, Girault J-A, Chan S, Kastner P, Canals JM. Helios expression coordinates the development of a subset of striatopallidal medium spiny neurons. Development. 2017. https://doi.org/10.1242/dev.138248.
61. Martín-Ibáñez R, Crespo E, Urbán N, Sergent-Tanguy S, Herranz C, Jaumot M, Valiente M, Long JE, Pineda JR, Andreu C, Rubenstein JLR, Marín Ó, Georgopoulos K, Mengod G, Fariñas I, Bachs O, Alberch J, Canals JM. Ikaros-1 couples cell cycle arrest of late striatal precursors with neurogenesis of enkephalinergic neurons. J Comp Neurol. 2010;518:329–51. https://doi.org/10.1002/cne.22215.
62. McGrath J, Saha S, Chant D, Welham J. Schizophrenia: a concise overview of incidence, prevalence, and mortality. Epidemiol Rev. 2008;30:67–76. https://doi.org/10.1093/epirev/mxn001.
63. Mendrek A, Mancini-Marïe A. Sex/gender differences in the brain and cognition in schizophrenia. Neurosci Biobehav Rev. 2016;67:57–78. https://doi.org/10.1016/j.neubiorev.2015.10.013.
64. Molnár A, Georgopoulos K. The Ikaros gene encodes a family of functionally diverse zinc finger DNA-binding proteins. Mol Cell Biol. 1994;14:8292–303. https://doi.org/10.1128/MCB.14.12.8292.
65. Momtazmanesh S, Zare-Shahabadi A, Rezaei N. Cytokine alterations in schizophrenia: an updated review. Front Psychiatry. 2019. https://doi.org/10.3389/fpsyt.2019.00892.
66. Moyer CE, Shelton MA, Sweet RA. Dendritic spine alterations in schizophrenia. Neurosci Lett. 2015;601:46–53. https://doi.org/10.1016/j.neulet.2014.11.042.
67. Nelson TE, Gruol DL. The chemokine CXCL10 modulates excitatory activity and intracellular calcium signaling in cultured hippocampal neurons. J Neuroimmunol. 2004;156:74–87. https://doi.org/10.1016/j.jneuroim.2004.07.009.
68. O'Brien SM, Scully P, Dinan TG. Increased tumor necrosis factor-alpha concentrations with interleukin-4 concentrations in exacerbations of schizophrenia. Psychiatry Res. 2008;160:256–62. https://doi.org/10.1016/j.psychres.2007.11.014.
69. Potkin SG, Guffanti G, Lakatos A, Turner JA, Kruggel F, Fallon JH, Saykin AJ, Orro A, Lupoli S, Salvi E, Weiner M, Macciardi F. Hippocampal atrophy as a quantitative trait in a genome-wide association study identifying novel susceptibility genes for Alzheimer's disease. PLoS ONE. 2009;4:e6501. https://doi.org/10.1371/journal.pone.0006501.
70. Powell CM, Miyakawa T. Schizophrenia-relevant behavioral testing in rodent models: a uniquely human disorder? Biol Psychiatry. 2006;59:1198–207. https://doi.org/10.1016/j.biopsych.2006.05.008.
71. Quirion MR, Gregory GD, Umetsu SE, Winandy S, Brown MA. Cutting edge: ikaros is a regulator of Th2 cell differentiation. J Immunol. 2009;182:741–5. https://doi.org/10.4049/jimmunol.182.2.741.
72. Rabadan MA, De La Cruz ED, Rao SB, Chen Y, Gong C, Crabtree G, Xu B, Markx S, Gogos JA, Yuste R, Tomer R. An in vitro model of neuronal ensembles. Nat Commun. 2022;13:3340. https://doi.org/10.1038/s41467-022-31073-1.
73. Reimegård J, Tarbier M, Danielsson M, Schuster J, Baskaran S, Panagiotou S, Dahl N, Friedländer MR, Gallant CJ. A combined approach for single-cell mRNA and intracellular protein expression analysis. Commun Biol. 2021;4:624. https://doi.org/10.1038/s42003-021-02142-w.
74. Remington G. Book review: the schizophrenia spectrum. Can J Psychiatry. 2018;63:257–257. https://doi.org/10.1177/0706743718758042.
75. Remington G, Foussias G, Fervaha G, Agid O, Takeuchi H, Lee J, Hahn M. Treating negative symptoms in schizophrenia: an update. Curr Treat Options Psychiatry. 2016;3:133–50. https://doi.org/10.1007/s40501-016-0075-8.
76. Ribeiro-Santos R, Lucio Teixeira A, Vinicius Salgado J. Evidence for an immune role on cognition in schizophrenia: a systematic review. Curr Neuropharmacol. 2014;12:273–80. https://doi.org/10.2174/1570159X1203140511160832.
77. Rømer TB, Jeppesen R, Christensen RHB, Benros ME. Biomarkers in the cerebrospinal fluid of patients with psychotic disorders compared to healthy controls: a systematic review and meta-analysis. Mol Psychiatry. 2023;28:2277–90. https://doi.org/10.1038/s41380-023-02059-2.
78. Sada-Fuente E, Aranda S, Papiol S, Heilbronner U, Moltó MD, Aguilar EJ, González-Peñas J, Andreu-Bernabeu Á, Arango C, Crespo-Facorro B, González-Pinto A, Fañanás L, Arias B, Bobes J, Costas J, Martorell L, Schulze TG, Kalman JL, Vilella E, Muntané G. Correction: common

genetic variants contribute to heritability of age at onset of schizophrenia. Transl Psychiatry. 2023;13:369. https://doi.org/10.1038/s41398-023-02651-8.
79. Saha S, Chant D, Welham J, McGrath J. A systematic review of the prevalence of schizophrenia. PLoS Med. 2005;2: e141. https://doi.org/10.1371/journal.pmed.0020141.
80. Sancho-Balsells A, Borràs-Pernas S, Brito V, Alberch J, Girault J-A, Giralt A. Cognitive and emotional symptoms induced by chronic stress are regulated by EGR1 in a subpopulation of hippocampal pyramidal neurons. Int J Mol Sci. 2023;24:3833. https://doi.org/10.3390/ijms24043833.
81. Sancho-Balsells A, Brito V, Fernández B, Pardo M, Straccia M, Ginés S, Alberch J, Hernández I, Arranz B, Canals JM, Giralt A. Lack of helios during neural development induces adult schizophrenia-like behaviors associated with aberrant levels of the TRIF-recruiter protein WDFY1. Front Cell Neurosci. 2020;14:5. https://doi.org/10.3389/fncel.2020.00093.
82. Sanz H, Aponte JJ, Harezlak J, Dong Y, Ayestaran A, Nhabomba A, Mpina M, Maurin OR, Díez-Padrisa N, Aguilar R, Moncunill G, Selidji Todagbe A, Daubenberger C, Dobaño C, Valim C. drLumi: An open-source package to manage data, calibrate, and conduct quality control of multiplex bead-based immunoassays data analysis. PLoS ONE. 2017;12: e0187901. https://doi.org/10.1371/journal.pone.0187901.
83. Schizophrenia Working Group of the Psychiatric Genomics Consortium. Biological insights from 108 schizophrenia-associated genetic loci. Nature. 2014;511:421–7. https://doi.org/10.1038/nature13595.
84. Schwarz MJ, Krönig H, Riedel M, Dehning S, Douhet A, Spellmann I, Ackenheil M, Möller H-J, Müller N. IL-2 and IL-4 polymorphisms as candidate genes in schizophrenia. Eur Arch Psychiatry Clin Neurosci. 2006;256:72–6. https://doi.org/10.1007/s00406-005-0603-9.
85. Schwarz MJ, Müller N, Riedel M, Ackenheil M. The Th2-hypothesis of schizophrenia: a strategy to identify a subgroup of schizophrenia caused by immune mechanisms. Med Hypotheses. 2001;56:483–6. https://doi.org/10.1054/mehy.2000.1203.
86. Sen P, Kemppainen E, Orešič M. Perspectives on systems modeling of human peripheral blood mononuclear cells. Front Mol Biosci. 2018. https://doi.org/10.3389/fmolb.2017.00096.
87. Shevchenko A, Tomas H, Havli J, Olsen JV, Mann M. In-gel digestion for mass spectrometric characterization of proteins and proteomes. Nat Protoc. 2006;1:2856–60. https://doi.org/10.1038/nprot.2006.468.
88. Şimşek Ş, Yıldırım V, Çim A, Kaya S. Serum IL-4 and IL-10 Levels correlate with the symptoms of the drug-naive adolescents with first episode, early onset schizophrenia. J Child Adolesc Psychopharmacol. 2016;26:721–6. https://doi.org/10.1089/cap.2015.0220.
89. Sonnenschein SF, Gomes FV, Grace AA. Dysregulation of midbrain dopamine system and the pathophysiology of schizophrenia. Front Psychiatry. 2020. https://doi.org/10.3389/fpsyt.2020.00613.
90. Sperner-Unterweger B, Whitworth A, Kemmler G, Hilbe W, Thaler J, Weiss G, Fleischhacker WW. T-cell subsets in schizophrenia: a comparison between drug-naive first episode patients and chronic schizophrenic patients. Schizophr Res. 1999;38:61–70. https://doi.org/10.1016/S0920-9964(98)00175-3.
91. Sullivan PF. Questions about DISC1 as a genetic risk factor for schizophrenia. Mol Psychiatry. 2013;18:1050–2. https://doi.org/10.1038/mp.2012.182.
92. Sun Y, Koyama Y, Shimada S. Inflammation from peripheral organs to the brain: how does systemic inflammation cause neuroinflammation? Front Aging Neurosci. 2022. https://doi.org/10.3389/fnagi.2022.903455.
93. Sutley-Koury SN, Taitano-Johnson C, Kulinich AO, Farooq N, Wagner VA, Robles M, Hickmott PW, Santhakumar V, Mimche PN, Ethell IM. EphB2 signaling is implicated in astrocyte-mediated parvalbumin inhibitory synapse development. J Neurosci. 2024;44: e0154242024. https://doi.org/10.1523/JNEUROSCI.0154-24.2024.
94. Szlachta M, Pabian P, Kuśmider M, Solich J, Kolasa M, Żurawek D, Dziedzicka-Wasylewska M, Faron-Górecka A. Effect of clozapine on ketamine-induced deficits in attentional set shift task in mice. Psychopharmacology. 2017;234:2103–12. https://doi.org/10.1007/s00213-017-4613-x.
95. Tamminga CA, Buchanan RW, Gold JM. The role of negative symptoms and cognitive dysfunction in schizophrenia outcome. Int Clin Psychopharmacol. 1998;13:S21–6. https://doi.org/10.1097/00004850-199803003-00004.
96. Tyanova S, Temu T, Sinitcyn P, Carlson A, Hein MY, Geiger T, Mann M, Cox J. The Perseus computational platform for comprehensive analysis of (prote)omics data. Nat Methods. 2016;13:731–40. https://doi.org/10.1038/nmeth.3901.
97. Uhlhaas PJ, Singer W. Abnormal neural oscillations and synchrony in schizophrenia. Nat Rev Neurosci. 2010;11:100–13. https://doi.org/10.1038/nrn2774.
98. Valero M, de la Prida LM. The hippocampus in depth: a sublayer-specific perspective of entorhinal–hippocampal function. Curr Opin Neurobiol. 2018;52:107–14. https://doi.org/10.1016/j.conb.2018.04.013.
99. van Mierlo HC, Schot A, Boks MPM, de Witte LD. The association between schizophrenia and the immune system: review of the evidence from unbiased 'omic-studies.' Schizophr Res. 2020;217:114–23. https://doi.org/10.1016/j.schres.2019.05.028.
100. Venturino A, Schulz R, De Jesús-Cortés H, Maes ME, Nagy B, Reilly-Andújar F, Colombo G, Cubero RJA, Schoot Uiterkamp FE, Bear MF, Siegert S. Microglia enable mature perineuronal nets disassembly upon anesthetic ketamine exposure or 60-Hz light entrainment in the healthy brain. Cell Rep. 2021;36:109313. https://doi.org/10.1016/j.celrep.2021.109313.
101. Wang J-H, Nichogiannopoulou A, Wu L, Sun L, Sharpe AH, Bigby M, Georgopoulos K. Selective defects in the development of the fetal and adult lymphoid system in mice with an ikaros null mutation. Immunity. 1996;5:537–49. https://doi.org/10.1016/S1074-7613(00)80269-1.
102. Wegrzyn D, Juckel G, Faissner A. Structural and functional deviations of the hippocampus in schizophrenia and schizophrenia animal models. Int J Mol Sci. 2022;23:5482. https://doi.org/10.3390/ijms23105482.
103. Wu JQ, Green MJ, Gardiner EJ, Tooney PA, Scott RJ, Carr VJ, Cairns MJ. Altered neural signaling and immune pathways in peripheral blood mononuclear cells of schizophrenia patients with cognitive impairment: a transcriptome analysis. Brain Behav Immun. 2016;53:194–206. https://doi.org/10.1016/j.bbi.2015.12.010.
104. Wu W, Nelson GM, Koch R, Donovan KA, Nowak RP, Heavican-Foral TB, Nirmal AJ, Liu H, Yang L, Duffy J, Powers F, Stevenson KE, Jones MK, Ng SY, Wu G, Jain S, Xu R, Amaka S, Trevisani C, Donaldson NL, Hagner PR, de Leval L, Gaulard P, Iqbal J, Thakurta A, Fischer ES, Adelman K, Weinstock DM. Overcoming IMiD resistance in T-cell lymphomas through potent degradation of ZFP91 and IKZF1. Blood. 2022;139:2024–37. https://doi.org/10.1182/blood.2021014701.
105. Xiao J, Zhou H, Wu N, Wu L. The non-canonical Wnt pathway negatively regulates dendritic cell differentiation by inhibiting the expansion of Flt3+ lymphocyte-primed multipotent precursors. Cell Mol Immunol. 2016;13:593–604. https://doi.org/10.1038/cmi.2015.39.
106. Xie S, Wei H, Peng A, Xie A, Li J, Fang C, Shi F, Yang Q, Huang H, Xie H, Pan X, Tian X, Huang J. Ikzf2 regulates the development of ICOS+ Th cells to mediate immune response in the spleen of S. japonicum-Infected C57BL/6 Mice. Front Immunol. 2021. https://doi.org/10.3389/fimmu.2021.687919.
107. Zhang T, Zeng J, Wei Y, Ye J, Tang X, Xu L, Hu Y, Cui H, Xie Y, Tang Y, Liu X, Liu H, Chen T, Li C, Wang J. Changes in inflammatory balance correlates with conversion to psychosis among individuals at clinical high-risk: A prospective cohort study. Psychiatry Res. 2022;318:114938. https://doi.org/10.1016/j.psychres.2022.114938.
108. Zhu M, Liu Z, Guo Y, Sultana MS, Wu K, Lang X, Lv Q, Huang X, Yi Z, Li Z. Sex difference in the interrelationship between TNF-α and oxidative stress status in first-episode drug-naïve schizophrenia. J Neuroinflammation. 2021;18:202. https://doi.org/10.1186/s12974-021-02261-5.

Publisher's Note